Charles University of Prague
Faculty of Mathematics and Physics

Master's thesis

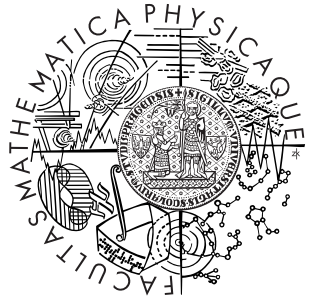

Jiří Klimeš

Inelastic transmission of current through molecular bridge

Department of Chemical Physics and Optics

Supervisor: RNDr. Martin Čížek, PhD,
Institute of Theoretical Physics
Area of study: Chemical Physics

2007

I would like to thank my supervisor RNDr. Martin Čížek, PhD, for his help throughout my work. I am also grateful to people from the $\mathcal{META}$CENTRUM project that allowed me to use their facilities for my calculations. I am thankful to my parents for their support throughout my studies.

I hereby state that I have written this master's thesis by myself using only the cited references. I agree to lend it.

Prague, 20. 4. 2007 Jiří Klimeš

Contents

Název práce: Neelastický průchod proudu molekulárním mostem
Autor: Jiří Klimeš
Katedra: Katedra chemické fyziky a optiky
Vedoucí práce: RNDr. Martin Čížek, PhD, Ústav teoretické fyziky
e-mail vedoucího: cizek@mbox.troja.mff.cuni.cz

Abstrakt:

Molekulární elektronika je jednou z možných nástupců současných technologií výroby elektronických součástek. Experimentálně už byly sestaveny základní prvky jako tranzistor nebo dioda, kde aktivním prvkem byla jediná molekula. Současně se také zpřesňuje teoretický popis těchto systémů – molekulárních můstků. V této práci jsme se zaměřili na výpočty vlastností techto systémů na úrovni modelu neortogonální těsné vazby. Zejména jsme se zaměřili na vliv elektrody na elektronové hustoty v kontaktu, které mají významný vliv na transportní vlastnosti. Dále jsme provedli výpočty transmisních funkcí pro vybrané systémy. Byl implementován postup, který umožňuje provést výpočet pro různá napětí. Naše numerické procedury umožňují nahrazení těsnovazebného popisu přesnějšími *ab initio* metodami. Výsledky mohou být dále použity jako vstup pro popis neelastických efektů při průchodu elektronu můstkem.
Keywords: Molekulární elektronika, Těsnovazebný model, Kvantový transport.

Title: Inelastic transmission of current through molecular bridge
Author: Jiří Klimeš
Department: Department of Chemical Physics and Optics
Supervisor: RNDr. Martin Čížek, PhD, Institute of Theoretical Physics
Supervisor's e-mail address: cizek@mbox.troja.mff.cuni.cz

Abstract:

Molecular electronics is one of the possible successor of the contemporary technologies of production of electronic devices. Basic devices, such as transistor or diode, where single molecule acted as the active element, were demonstrated experimentally in the past decade. Theoretical description of these systems – molecular bridges – improves at the same time. In this work we focused on calculation of properties of such systems at the level of non-orthogonal tight binding model. In particular we studied the influence of electrodes on the electron densities in the contact as these play an important role for the transport. In addition we calculated transmission functions for selected systems under different biases. Our numerical codes allow replacement of the tight-binding level with more accurate *ab initio* methods and the results can be further used as an input for the description of inelastic effects during electron transmission.
Keywords: Molecular electronics, Tight-binding model, Quantum transport.

Chapter 1

Introduction

Miniaturization in the industry in the past decades has enabled incredible improvements of electronic devices. Continuous demand for faster, lighter and cheaper gadgets stimulates the research of semiconductors on the submicron scale and new ways are exploited to bring the industry to the atomic scale. This scale-down brings lower power consumption that allows production of more complicated devices in higher amounts. The progress can be illustrated with a famous example – the long-standing Moore's law of the computer industry – roughly every eighteen months the number of transistors in a computer chip is doubled. Gordon Moore found out this dependence in 1964 for the computer microchips but it seems to be valid for many different devices and various fields of technology. The development of this field can be shown in a simple way: this thesis is written on a computer with processor made with 130nm technology, where the number denotes the width of the transistor gate. Intel plans to start production of computer processors made with transistors three times thiner during this year. The edge of the silicon based technologies around 20nm is to be reached in the next ten years using extreme lithography techniques. However, the way further seems to be closed because the technique depends on a laser source of appropriate wavelength and usage of novel materials. There are many ideas how to prolongate the validity of the Moore's law after the possible ending of the silicon era, for example, people try to force the silicon to emit light, which would allow construction of optical chips. There are also some completely new approaches like quantum computing.

Scientists are able to produce layered semiconductor nanostructures, where the electron wave function is confined into two dimensions. This 2-dimensional electron gas (2DEG) can be further restricted with applied electric field to form only zero-dimensional structure – a quantum dot. Various interesting physical phenomena such as Coulomb blockade and quantum Hall effect have been observed in these systems. The Coulomb blockade is an important quantum effect appearing when a flow of the current through the quantum dot is blocked by other electron occupying the dot. It was also confirmed that the conductance is in this small systems quantized with an unit $2e^2/h$. Very interesting applications have been constructed, for example alternate current device that allows exactly one electron to pass through it during one period, having impact in metrology.

This fast development of the research on the nanoscale would not be possible without

some inventions, the most important of them maybe was the scanning tunneling microscope (STM) – device where a sharp tip is used to study surface properties. It was constructed in 1982 (Binning *et al.* (1982)) and awarded with the Nobel price four years thereafter. The researchers were able to measure a current between the tip and the surface and feel the individual atoms for the first time. Later the variant for non-conducting surfaces – the atomic force microscope (AFM) – was constructed allowing also to push the atoms on the surface. This was demonstrated by formation of the letters IBM written on a surface with individual atoms. However, cryogenic temperatures were needed and only recently the Japanese scientists were able to form the letters Si on a surface at room temperature.

Another important invention that will allow future miniaturization were the discoveries of various forms of carbon – fullerens in 1985 and the carbon nanotubes in 1991. These play an important role in the possible descendant of the silicon technology – the molecular electronics (ME) (Heath and Ratner (2003)). In this approach the active elements like transistors and diodes are made of molecules or nanotubes. Although there is still a long way to a functional ME chip, the first active elements have been demonstrated in the past decade. As a very recent example we mention a single organic molecule transistor. Molecule used to construct the device has two distinct parts: an aliphatic chain and a part with conjugated bonds. The part of the molecule with conjugated bonds was connected to two carbon nanotubes acting as a source and a drain and another carbon nanotube was connected to the long aliphatic chain of the molecule serving as a gate. Carbon nanotubes have interesting electronic properties depending on the structure of the nanotube. They can act as a metal, semi-metal or semiconductor. Besides of their electronic properties they have a large area of other future applications because of their weight to stress ratio.

The progress is very promising but there are still many steps to be figured out, one of which is how to connect the single pieces together to form a chip in series. The contemporary and previous technologies are based on a top-bottom approach – macroscopic devices construct microdevices. Completely different approach represent a bottom-up construction presented in 1981 by K. E. Drexler. The main idea is that macroscopic devices would be made – assembled – by nanodevices. This is not a new idea – nature does work in this way for a long time in the bodies of living organisms: we are all assembled by proteins in accordance with our DNA. Many possible variants of the bottom-up approach have been proposed, for example self-assembly techniques employing modified proteins or use of the natural pairing of the double strand structure of the DNA. Single strands would be synthesised and then mixed to form three dimensional structure, which would be used as a skeleton for the circuits.

Other important issue that has to be solved is the effect of vibrations and temperature on the active elements. Molecular vibrations strongly influence the properties of the molecular electronic devices and large currents can lead to excitations of higher vibrational states and to a breakdown of the device. On the other hand, some devices that would exploit the vibrations in a positive way were proposed, therefore it is important to understand the effects of vibrations before constructing a device. Theoretical pre-concepts of this issue come from the studies of molecular layers in the inelastic electron transmis-

sion spectroscopy (IETS, for overview see Hansma (1977)). The setup is very similar to the basic ME experiments – one measures current-voltage characteristics of the molecular layer between two leads. It was found that for some voltages the electron in IETS can undergo an inelastic scattering and can be backscattered. This lowers the current and results in a step in a differential conductance spectra. Similar situation can happen for a single molecule between two leads (Stipe *et al.* (1998) for STM-C_2H_2-surface) and also for atomic wires (wire with one atom in cross-section) made of, for example, gold (Agraït *et al.* (2002)).

In all potential applications the quantum transport of electrons across the active elements of atomic or molecular size must be understood. This goal was addressed by recent transport experiments. In the following paragraphs we are going to focus on 1D atomic wires and organic molecules.

1.1 Atomic wires

The atomic wire experiments were predated by point contact experiments, where the contact was formed by approximately hundreds of atoms. Already in these systems a non-ohmic behaviour was found. Point contact experiments have also provided information about interactions of electrons with phonons and other excitations (for overview see Jansen *et al.* (1980)), the method is called a point-contact spectroscopy. Similarly to the IETS, the incoming electrons can emit a phonon and be backscattered. The backscattered electrons reduce the current and therefore the conductance. This effect can be seen as a peak in the differential conductance spectrum. Energy of the electron has to be sufficiently high to emit the phonon, thus this happens for a bias higher or equal to the phonon energy.

The ultimate version of the point contact experiment is the atomic point contact constructed with the STM – here only one atom can be between the tip and the surface. Moreover, for some metals it is possible to form an atomic wire between the tip and the surface (Fig 1.1). The STM device can work in two different regimes: when the distance of the tip to the surface is large, only tunneling current occurs. When the tip is driven

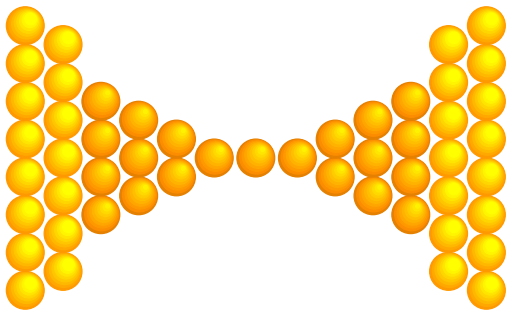

Figure 1.1: Simplistic visualization of an atomic wire formed in a contact of two leads. Only part of the surfaces of the right and left leads are shown.

towards the surface, the overlap of the electronic wave functions raises and in some distance, the tip touches the surface. It was found that conductance of many materials in this state equals to integer multiple of the unit quantum conductance $2e^2/h$. In that case the so-called quantum conductance channel is opened. The transformation from the vacuum regime to the contact regime was firstly studied by Gimzewski and Möller (1987).

Further experiments studied formation of the contact for various materials. For example, Dürig *et al.* (1990) used Ir tip and surface to study periodical formation of the contact. Agraït *et al.* (1993) studied changes between contact regime with single quantum conductance and almost zero conductance in the vacuum regime for vibrating tip.

Another experiments were done using a mechanically controllable break junction (MCBJ). In this device metal is placed on a flexible bending beam and the beam is bended until the metal forms the atomic contact. Using MCBJ Muller *et al.* (1992a, 1992b) found conductance steps in Pt atom size point contacts. These steps in the conductance for increasing distance were also found for Cu and Al contacts (Krans *et al.* (1993)). These experiments pointed at a formation of an atomic wire. Further experiments studied the current-voltage characteristics, for instance, Nielsen *et al.* (2002) studied differences in the conductances of Au and Pt and found ohmic behaviour for Au and non-ohmic for the Pt contacts.

Long atomic wires of gold were studied by Agraït *et al.* (2002), they were able to form an atomic wire with length of 22 Å using the STM device. The zero bias conductance during the measurement was found to be approaching quantum unit with increasing length of the wire. What was more important, the conductance stepped down after the bias exceeded energy of a vibration.

The stability and conductance of atomic wires were studied theoretically using various methods within the framework of the quantum mechanics and classic molecular dynamics. Over the years the studies shifted from molecular dynamics simulations to more sophisticated *ab initio* methods. Bratkovsky *et al.* (1995) performed molecular dynamics simulation of nickel contact. They studied its stability and also calculated its conductance from equations of the quantum mechanics. The first *ab initio* calculations of conductances of Al atomic wires were done by Lang (1995), he used simple jeelium model to describe the electrodes. The conductance of Al and Nb point contacts using tight-binding model was studied by Cuevas *et al.* (1998). In agreement with experiments, they found different conductances about 3 (5) $2e^2/h$ for Al (Nb). Similar calculations on gold at the tight-binding level were done by Brandbryge *et al.* (1999). They studied conductance of gold atomic wires with up to 6 atoms which was found to be near the quantum unit. Mozos *et al.* (2002) studied Au and Ag nanowires using TRANSIESTA code with implementation of the NEGF-DFT algorithm. Further simulations at the DFT level studied the stability of the nanowires during the breaking of the contact (Jelínek *et al.* (2003) on Al, Dreher *et al.* (2005) on Au).

1.2 Molecules

Conductance of single molecules have been studied with similar experimental techniques as the conductance of the atomic wires: STM and MCBJ. Conductance of longer molecules such as carbon nanotubes can be also studied with mesoscopic electrodes obtained by nanolitography. Idealized structure of the experimental structure is shown in Fig. 1.2. Figure shows benzenedithiol (BDT) molecule that is widely used both experimentally and theoretically as a testing molecule.

Joachim and Gimzewski (1995) studied fulleren C_{60} adsorbed on a gold surface using the STM. In their experiment they were able to measure the current in the vacuum regime, during the contact of the tip with the molecule and the current through the molecule deformed with the tip. Furthermore, they were able to construct macroscopic amplifier based on a single C_{60} molecule (Joachim and Gimzewski (1997)).

The theoretical variant of IETS for single molecules and STM was given by Persson and Baratoff (1987), they predicted that the conductance should drop after opening of inelastic channel. The effect of vibrations was found experimentally by Stipe *et al.* (1998) on an acetylene molecule adsorbed on a copper surface. The influence of the vibration was positive, the conductance raised after the vibrational channel had opened. Measurements with different molecules during the last years show both increase and decrease of the current after an opening of a vibrational channel.

The studies found three important effects that influence the transport properties (Ness *et al.* (2001)): First, the strength of the interaction between the delocalized electronic states in the reservoir and the electronic states in the wire that extend along it. In this case the conductance raises with the interaction and moreover, larger interaction prevents the Coulomb blockade regime. Second, for small voltages and non-Coulomb blockade regime is the transport dominated by electrons tunneling through the HOMO-LUMO gap, while the conductance raises with decreasing gap. The third important factor is the influence of the potential profile along the junction and alignment of HOMO and LUMO relative to the Fermi levels in the reservoirs.

Among the study of single isolated molecules, monolayers of organic molecules were studied using STM. Bumm *et al.* (1996, 1999) studied conductance of molecules with

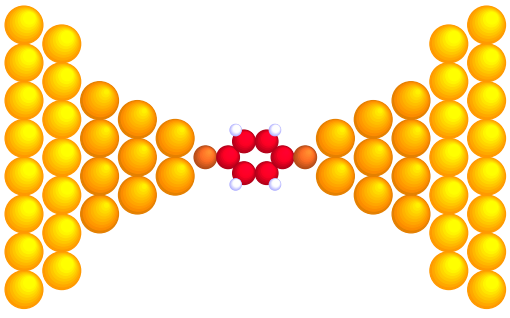

Figure 1.2: Simplistic view of a molecular junction with a BDT molecule.

conjugated bonds in self-assembled monolayers of alkane on a surface, and conductance of monolayers of organic molecules. Langlais *et al.* (1999) were able to measure the properties of molecular wires pointing out from step edges on the surface.

Using the mechanically controllable break junctions several groups were able to measure conductance of a very small number of molecules. The first reports on a measurement of conductance of BDT molecules in the MCBJ were published by Reed *et al.* (1997). They argued that the number of active molecules "could be as few as one".

Transport properties of the carbon nanotubes were measured using various experimental setups. First measurements of the conductance were done by the Bockrath *et al.* (1997) on the bundles of single wall carbon nanotubes (SWCN). They found conductance strongly dependent on temperature and gate voltage. Similar experiments on multi-wall carbon nanotubes (MWCN) were presented by Frank *et al.* (1998). Tans *et al.* (1998) constructed a room temperature field-effect transistor using carbon nanotube connected to two Pt electrodes. Temperature dependence of the conductance of the SWCN was also studied by Zhou *et al.* (2000) in a presence of a gate electrode that shifted the level of Fermi energy in the nanotube.

1.3 Calculations of current

The first theoretical calculations of properties of a molecular electronic device were presented by Aviram and Ratner (1974) on a molecule between two leads. They used treatment similar to the perturbation theory and showed that the molecule with donor and acceptor π systems can have properties of a rectifier. They calculated the transmission rates of electron in an applied external field from the donor site to the acceptor site. Since that time many approaches to the electron transport in molecular devices have been developed (Nitzan (2001), Nitzan and Ratner (2003)) and here we present the main of them.

The basic setup of the transport calculations was set by Landauer (1970). It views the current like elastic scattering of electrons from channels in one lead to the states of the second lead. The Landauer formula connects the transmission probabilities T_{ij} between two channels i and j with the total conductance

$$g = \frac{2e^2}{h} \sum_{ij} T_{ij} \,. \tag{1.1}$$

The value of T_{ij} lies between zero and one, zero means that the conductance channel is closed, while one means that the channel is opened. The resistance of wires with one open channel is $\sim 12.8\,\mathrm{k}\Omega$. This formula was generalized by Meir and Wingreen (1992) (and Jauho *et al.* (1994)) for the case of interacting region.

The electron transport can be understood as a scattering event that can be described with the scattering equations. The introduction to this approach can be found in Mujica *et al.* (1994), the first *ab initio* calculations were done by Lang (1995) for Al atomic wires and by Hirose and Tsukada (1995) for Na electrodes and tip structure. In this theory the

vibrational states of the molecule can be included in the calculation and probabilities of excitation of a vibrational state by the electron can be calculated. Comparison of current in molecular junctions with and without the vibrations was studied by Benesch *et al.* (2006).

Widely used approach to the calculation of transport in various systems uses the theory of non-equilibrium Green's functions. The relative simplicity of the final equation for transmission allows calculations of current for various Hamiltonians: from one level state between two electrodes to self-consistent *ab initio* DFT calculations. Vibrations can be also included in the model using the perturbation theory.

In the past years several groups have implemented the NEGF-DFT algorithm to study various systems: a metallic-nanotube contact (Taylor *et al.* (2001)), or a molecule between two leads (Xue *et al.* (2002, 2003)). Liang *et al.* (2004) studied the potential profiles in the junction in a presence of a gate electrode. The effect vibrations on Au atomic wires or organic molecules was studied by several groups (Frederiksen *et al.* (2004), Paulsson *et al.* (2005), Sergueev *et al.* (2005)). These papers also focus on the important issue of heating of the device. Many groups have developed their own implementations of the NEGF-DFT algorithms and there are many publications using this method.

Using the NEGF or scattering theories one usually tries to find the steady-state solution. The next step forward are the full time simulations, although these are computationally demanding. The important feature of the time dependent calculations is that we can study the behaviour of the system. Other important outcome of the time dependent analysis is the time-response of the device. This is because of the possible applications of the nanodevices as switches. The methods of the simulations range from molecular dynamics simulations with current calculated from quantum methods (Dreher *et al.* (2005)) to ab-initio simulations. For example, Jelínek *et al.* (2003) used DFT simulation and NEGF conductance formula to calculate the time dependency of current in Al (and later Au) point contacts during breaking of the contact. The approach of the time-dependent simulations was studied by Sánchez *et al.* (2006) using adiabatic local-density approximation (ALDA). However, the adiabatic methods do not describe properly the energy flows between electrons and ions. Some methods were proposed to correct this deficiency, for example correlated electron-ion dynamics method (CEID) (Horsfield *et al.* (2005)).

1.4 Motivation and aims of this work

For the future applications it is important to understand how different geometries of the contact electrode-molecule affect the transport through the molecule or atomic wire. This includes considerations of the effect of the electrodes on electronic states of the molecule. In many calculations, mostly of inelastic transport, no shift of the electronic levels is considered and another important parameter – density of states of the electrode – is often replaced by a simpler energy independent term. To asses the impact of this assumption we are interested in the differences between the transport properties in this approximation and with more realistic calculation of the electrode.

Particularly, we are interested in calculation of surface electronic properties of the electrodes, electronic properties of clusters of atoms (tips) placed on the surface and on transport properties of various contacts between two electrodes. To calculate this properties we

– implemented non-orthogonal tight-binding method

– implemented various techniques for calculation of Green's functions

– calculated the surface Green's function of semi-infinite lead.

These procedures allows us to calculate

– the effect of the surface on electronic states in the cluster of atoms and on the transport properties

– effect of the tip geometry on the electronic states in the tip and on the transport properties.

For the future work we are interested in the possibility of replacement of the tight-binding model with *ab initio* methods and in the inclusion of molecular vibrations. With these goals in mind the present calculations could be viewed as a test for implementation of more precise methods.

This thesis is organized as follows: This chapter gives summary of the experimental and theoretical results. Second chapter introduces the tight-binding model and its application to calculation of bulk and cluster properties. Basics of the Green's functions theory are presented in the third chapter. Methods of calculation of the surface Green's functions and details of the implementation are discussed in the fourth chapter. The calculation of electronic properties of different tips placed on surface is presented in chapter five. This is followed by evaluation of transmission functions for different systems in chapter six. The thesis is summarized in Concluding chapter.

Note that the atomic units are employed throughout this work, i.e. $\hbar = \mathrm{e} = 1$.

Chapter 2

Tight-Binding model

The first digital computers opened a way to calculations of electronic properties of polyatomic systems. Nevertheless, it was still necessary to develop approximations that describe well the calculated properties but simplify the time-consuming calculations. Slater and Koster (1954) introduced the tight-binding method that uses a simplified Hamiltonian in a basis of valence orbitals. The Hamiltonian elements are calculated from the atomic coordinates and symmetry of interacting orbitals using a set of parameters. Since the publication, the method has been widely used for large systems and also for calculations of bulk states in infinite periodical systems, where the Bloch functions are used. The method has many modifications, for overview see Goringe *et al.* (1997).

2.1 Calculation of Hamiltonian matrix elements

The evaluation of the Hamiltonian matrix elements is based on a two center approximation, the interaction of two atomic orbitals depends only on the position of these two orbitals and their symmetry. The situation is thus similar to the calculation of a diatomic molecule – there is no dependence on any third center. The Hamiltonian elements of this system are easily calculated in a basis of atomic orbitals defined in a local coordinate system that has one axis (z') aligned with the vector $\mathbf{R}$ connecting the centers of the atoms. In this coordinate system many Hamiltonian elements are zeroed because of the symmetry. The nonzero Hamiltonian elements depend only on angular momenta of the atomic orbitals, for example, interaction between orbitals $p_{z'}$ and s (centered on the first and second atom respectively) is nonzero and we can denote it as $(sp\sigma)$, here σ denotes the symmetry of the formed orbital. Now we can take a basis of atomic orbitals defined in the original coordinate system. Since the orbitals p_x, p_y, p_z in this basis can be expressed as linear combinations of orbitals $p_{x'}, p_{y'}, p_{z'}$ in the local basis, there must be a simple expression for the Hamiltonian elements in the original coordinate system in terms of the only nonzero matrix element $(sp\sigma)$. The expressions depend on the direction cosines l, m, n of the vector $\mathbf{R}$ and were tabulated by Slater and Koster (1954). In the following paragraphs we give examples of the expressions.

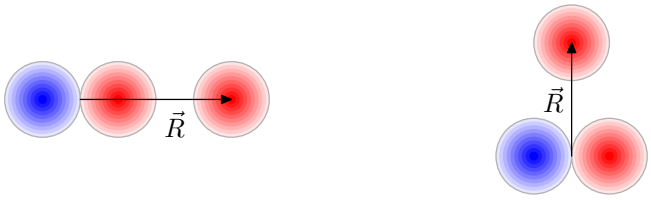

Figure 2.1: Interaction between s and p_x orbitals, maximal overlap to the left, zero interaction to the right. The angular dependence is $E_{s,x} = l(sp\sigma)$ and $E_{x,s} = -l(sp\sigma)$ because of the symmetry. The p_x function is odd whereas the s function is even.

Let us consider system of N atoms each with j orbitals with symmetry $s\,, p\,, \ldots$ on each atom of the system, we denote the orbitals as $\psi_{\alpha,\mathbf{R}_i}(\mathbf{r}) = \psi_\alpha(\mathbf{r}-\mathbf{R}_i)$, where $\alpha = s, p_x, p_y, \ldots$ is the type of orbital and $\mathbf{R}_i$ is its position. We have to evaluate interactions between every pair of $N \cdot j$ orbitals, although majority of the interactions will be small due to the distance and can be neglected. The actual number of orbitals per atom can differ according to the accuracy level and the problem one solves. As an example, we pick up two orbitals: s orbital located at $\mathbf{R}_i$ and p_x orbital centered at $\mathbf{R}_j$ (Fig. 2.1). To proceed we have to calculate the distance $R = |\mathbf{R}_i - \mathbf{R}_j|$ and direction cosines l, m, n between the two centres. The matrix element can be now evaluated with the use of the Slater and Koster table $\langle\psi_{s,\mathbf{R}_i}|H|\psi_{p_x,\mathbf{R}_j}\rangle = E_{s,x}(\mathbf{R}) = l(sp\sigma)$, where $(sp\sigma)$ is our value for the interaction of orbitals s and p forming σ bond in a distance R. We use the short hand notation of Slater and Koster to write x (y, z) for p_x (p_y, p_z) orbitals and similarly for d type orbitals.

The effect of the direction cosine l is that the interaction is repulsive when the overlap is negative and that the interaction vanishes for s orbital placed in the zero plane of the p_x orbital (Fig. 2.1, right). In this configuration the molecular orbital σ is formed by the combination of p_z (or p_y) and s atomic orbitals.

As example of more complicated term, let us conceive two p_x orbitals (Fig. 2.2), where the matrix element is evaluated as

$$E_{x,x}(\mathbf{R}) = l^2(pp\sigma) + (1 - l^2)(pp\pi)\,. \tag{2.1}$$

Here is the interaction divided into the σ and π type orbital and the equation represents our imagination of the interaction: when the two orbitals lie on the same line they can form σ-(anti-)bond, when they lie next to each other they form π-bond. The interaction thus gradually changes between these two types. Because of the symmetry there is no dependence on the m and n direction cosines.

2.2 Non-orthogonal Tight-Binding

The original method of Slater and Koster used a set of orthogonal orbitals. In our calculations we use a method of Mehl and Papaconstantopoulos (1994) that uses a non-orthogonal

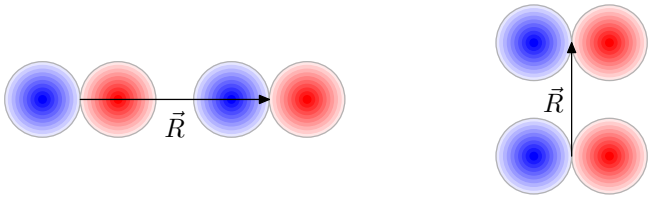

Figure 2.2: Interaction between two p_x orbitals, σ-anti-bond type to the left, π-bond type to the right. For p functions it is $E_{x,y} = E_{y,x}$, as we have two odd functions.

set of orbitals. The method was derived from the density functional theory (DFT) but the same equations for interactions as in the original tight-binding can be used.

The Hamiltonian consists of diagonal on-site elements h_{ii} and interaction elements h_{ij}. The overlap matrix S can be also divided into the on-site part and overlap elements between two orbitals on different sites. The on-site elements of the Hamiltonian are calculated using a density ρ_i, parameter that is calculated for each atom i and depends on the presence of other atoms in the vicinity of it. Each atom j that is closer to the atom i than a cutoff distance contributes to the density of the atom i with an exponentially decreasing factor, so that the final density is

$$\rho_i = \sum_{j \neq i} \exp[-\lambda^2 R_{ij}] F_c(R_{ij}) \,, \tag{2.2}$$

where R_{ij} is the distance between the two atoms and $F_c(R) = \{1 + \exp[(R - R_0)/l_0]\}^{-1}$ is the cutoff function depending on parameters R_0 and l_0. (For model of gold investigated further these parameters are $R_0 = 12.5$ a.u. and $l_0 = 0.25$ a.u..)

Using the density, the on-site elements are calculated as

$$h_{i\alpha} = a_\alpha + b_\alpha \rho_i^{2/3} + c_\alpha \rho_i^{4/3} + d_\alpha \rho_i^2 \,, \tag{2.3}$$

where i denotes the atom and α is the type of the orbital. The on-site elements are the same for all orbitals with the same angular momentum. The orbitals on each atom are taken to be normalized and having zero overlap between each other, therefore the on-site part of the overlap matrix S is taken to be the identity matrix.

The overlap and Hamiltonian parameters that enter the calculation of the nondiagonal matrix elements of overlap and Hamiltonian matrices are functions of distance as

$$(\gamma)(R) = (e_\gamma + f_\gamma R + \bar{f}_\gamma R^2) \exp[-g_\gamma^2 R] F_c(R) \,, \tag{2.4}$$

where γ represents the various type of interaction, e.g. $sp\sigma$, $sd\pi$ (see eq. 2.1) and e_γ, f_γ, $\bar{f}_\gamma$ and g_γ are fitted parameters for that type of interaction. Again the range of the interaction is limited with the cutoff function. The formula 2.4 with different set of parameters is also used for calculation of the overlap matrix. Now we can calculate arbitrary matrix element between two orbitals using results of 2.4 multiplied by appropriate combinations of the

direction cosines from the Table 1 from the paper of Slater and Koster as explained in the previous section.

The parameters of this method were determined to reproduce *ab initio* density functional results, they are available for more than 30 chemical elements. For FCC gold the method uses a set of nine orbitals, $5d$, $6s$ and $6p$. The total number of parameters to fit is 93. The files with parameters can be downloaded from the web pages of the authors (see the reference Mehl and Papaconstantopoulos (1996)).

2.2.1 Self-consistent Tight-Binding Method

One of the many variants of the tight-binding is the self-consistent tight binding. It assumes the local charge neutrality (LCN), condition, that each atom has a neutral charge. This is reasonable in the case of metals because the valence electrons are almost free to move within the crystal. To ensure this assumption, local potential is added to each atom, so that the Hamiltonian takes the form of $H = H_0 + e\Phi$. To calculate the potential shifts we need to calculate the local density of states on each atom. This, as we will show later, can be obtained from the Green's function method. By integration of the local density up to the Fermi level we obtain the local number of (valence) electrons. If the number of valence electrons is higher than the number for neutral atom, the atom has negative charge. In this case, potential is added to shift the electron levels to higher energies and lower the number of electrons under the E_{F}. The local potentials have to be calculated self-consistently.

Following the steps of Brandbyge *et al.* (1999), we use a shift potential matrix of the form

$$\Phi_{ij} = S_{ij}(\phi_i + \phi_j)/2\,, \tag{2.5}$$

where the indices i and j are indices of atoms. This form ensures constant shift of eigenvalues when we set $\phi_i = \phi$ for each i.

2.3 Cluster

For the first calculations we took a small cluster of gold atoms in the face-centered cubic structure. The purpose of this calculation is to compare a histogram of density of states of the cluster with a density of states of an infinite crystal (obtained with a calculation in the **k**-space, next section). The two plots should have the same characteristics and be the same for an infinite cluster. However, this calculation is restricted with the total number of atoms that can be used and also influence of the surface cannot be neglected when comparing the two plots.

The Hamiltonian and overlap matrices are computed in a straightforward way using the equations above. For the system we therefore get the generalised eigenvalue problem

$$Hc = ESc\,. \tag{2.6}$$

This equation can be transformed to the ordinary eigenvalue problem if we transform the basis as $c' = S^{1/2}c$. Then

$$HS^{-1/2}S^{1/2}c = ES^{1/2}S^{1/2}c \tag{2.7}$$

$$S^{-1/2}HS^{-1/2}S^{1/2}c = ES^{1/2}c \tag{2.8}$$

$$\tilde{H}c' = Ec' \,. \tag{2.9}$$

This problem of finding the transformation can be solved with standard methods, in our calculations we used the LAPACK library. The $S^{1/2}$ matrix can be found using an unitary transformation matrix U that diagonalises the overlap matrix $S_d = U^{-1}SU$, where $[S_d]_{ij} = s_i\delta_{ij}$. Then it is $S^{1/2} = US_d^{1/2}U^{-1}$, where $[S_d^{1/2}]_{ij} = \delta_{ij}\sqrt{s_i}$. Note that $s_i > 0$ since S must be positive definite. Finally, we find the eigenvalues of the transformed Hamiltonian $\tilde{H} = S^{-1/2}HS^{-1/2}$.

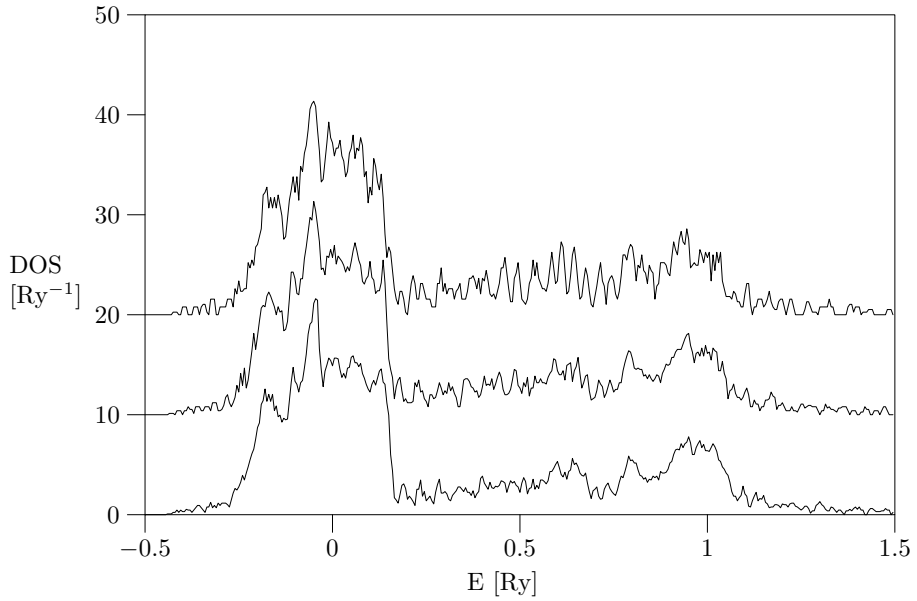

Figure 2.3: Density of states for cubic clusters containing 864 (bottom), 500 and 256 (top) atoms. The graphs are histograms of the eigenvalues. The main band around $E = 0$ belongs to d electrons, next to higher energies is wide s-band around the Fermi energy ($E_{\mathrm{F}} = 0.285$Ry in bulk) and approximately from 0.5 to 1.5 lies the p-band.

We calculated eigenvalues for clusters containing up to 864 gold atoms in the FCC lattice with lattice constant $a = 7.7099$ a.u., which is the lattice constant for bulk structure of gold. The lattice was constructed as a set of points in the space with coordinates $r = a/2(ix + jy + kz)$, where $i + j + k$ is an even number, this condition places the atoms into the points of the FCC lattice. Each of the numbers i, j and k was in absolute value lower than n, where n ranged from 7 (256 atoms) to 11 (864 atoms). The histograms of

the density of states for three different clusters are shown in Fig 2.3. The data on the plot were shifted and smoothed with a boxcar average with their neighbours.

If the rules of Slater and Koster (as explained in section 2.1.) are properly implemented, the eigenvalues should not depend on the orientation of the cluster in the space. To verify this invariance we calculated the eigenvalues of a small cluster containing 63 atoms, rotated in the space into various directions. The calculated values coincide at least on the first ten digits.

2.4 Electronic band structure

Infinite periodic potential problem in solid can be solved using the Bloch method. We consider a cubic cell in the crystal with N atoms. From the chosen set of orbitals on each atom ψ_α a linear combination

$$\varphi_{\mathbf{k}\,\alpha}(\mathrm{r}) = N^{-1/2} \sum_{\mathbf{R}_i} \exp(\mathrm{i}\,\mathbf{k}\cdot\mathbf{R}_i)\psi_\alpha(\mathbf{r}-\mathbf{R}_i) \tag{2.10}$$

is made, where N is number of atoms in one cell. In this new basis, the Hamiltonian is block-diagonalized in $\mathbf{k}$ and the eigenvalue problem can be solved for each $\mathbf{k}$ separately. The rank of the blocks in the Hamiltonian (and the overlap matrix) is equal to the number of basis functions on one atom. In our case of *spd* basis, we have blocks 9x9. The matrix elements between two Bloch sums read

$$H\alpha\beta(\mathbf{k}) = \langle\varphi_{\mathbf{k}\,\alpha}|H|\varphi_{\mathbf{k}\,\beta}\rangle = N^{-1} \sum_{\mathbf{R}_i,\,\mathbf{R}_j} \exp(\mathrm{i}\,\mathbf{k}\cdot(\mathbf{R}_j-\mathbf{R}_i)) \int \psi^*_\alpha(\mathbf{r}-\mathbf{R}_i) H \psi_\beta(\mathbf{r}-\mathbf{R}_j)\,\mathrm{d}V \tag{2.11}$$

where the sum is over N unit cells. Having a periodic crystal one summation can be eliminated because we have N equal contributions

$$H_{\alpha\beta}(\mathbf{k}) = \sum_{\mathbf{R}_j} \exp(\mathrm{i}\,\mathbf{k}\cdot(\mathbf{R}_j-\mathbf{R}_i)) \int \psi^*_\alpha(\mathbf{r}-\mathbf{R}_i) H \psi_\beta(\mathbf{r}-\mathbf{R}_j)\mathrm{d}V\,. \tag{2.12}$$

Notice that the two center interaction integrals can be computed only once, the only thing that changes in the Hamiltonian is the prefactor of the parts of the sum. Because of the translational invariance we can set $\mathbf{R}_i = 0$ and the equation further simplifies as

$$H_{\alpha\beta}(\mathbf{k}) = \sum_{\mathbf{R}_j} \exp(\mathrm{i}\,\mathbf{k}\cdot\mathbf{R}_j) E_{\alpha,\beta}(\mathbf{R}_j)\,. \tag{2.13}$$

The matrix elements for $\mathbf{R}_j = 0$ are the on-site elements h_α, so that the final equation reads

$$H_{\alpha\beta}(\mathbf{k}) = \delta_{\alpha\beta} h_\alpha + \sum_{\mathbf{R}_j \neq 0} \exp(\mathrm{i}\,\mathbf{k}\cdot\mathbf{R}_j) E_{\alpha,\beta}(\mathbf{R}_j)\,, \tag{2.14}$$

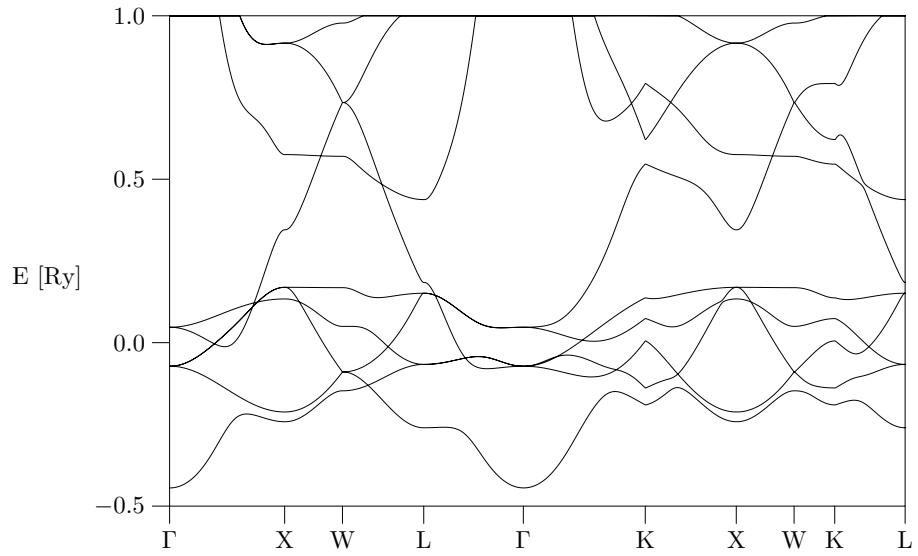

Figure 2.4: Energy bands of bulk gold over symmetry points in the first Brillouin zone. For the notation of the points we refer reader to standard books of solid state physics.

Using localised orbitals $\psi_\alpha(\mathbf{r} - \mathbf{R}_i)$ the interaction and overlap has a finite range therefore there is a finite number of integrals to evaluate. The overlap part is calculated in a similar way

$$S_{\alpha\beta}(\mathbf{k}) = \delta_{\alpha\beta} + \sum_{\mathbf{R}_j \neq 0} \exp(\mathrm{i}\,\mathbf{k}\cdot\mathbf{R}_j) S_{\alpha,\beta}(\mathbf{R}_j)\,. \tag{2.15}$$

The band structure is visualised as usual plotting of the eigenvalues of the Hamiltonian along various lines in the $\mathbf{k}$-space. We place a set of points on the lines $\mathbf{k}_n$ and the eigenvalue problem 2.6 is solved for each $\mathbf{k}_n$ with the Hamiltonian 2.14 and overlap matrix 2.15. For the calculation of matrix elements and density we took a box containing 365 atoms and calculated the density parameter for the central atom. We checked that the number of atoms was sufficiently large to include all the contributions. The non-orthogonal problem was orthogonalized with the $S^{-1/2}$ matrix as was shown in the previous section and the eigenvalues were calculated. The band structure is shown in Fig. 2.4, where the horizontal axis is labeled with the signs of points with special symmetry.

To obtain the density of states we discretize the values of $\mathbf{k}$ using Born-von Karman periodic boundary condition and we calculate nine eigenvalues for each $\mathbf{k}$ from a part of the $\mathbf{k}$-space that is equivalent to one quarter of the 1st Brillouin zone. We collect the data from all the points and use them to plot a histogram of the DOS. We used a part of one octant of the Brillouin zone that is four times larger than the first irreducible zone but allows better parametrization because of its cubic shape. The density is in Fig. 2.5, eigenvalues were calculated in 64000 points. From this DOS we found that the Fermi energy of the model equals $E_F = 0.285$ Ry. The DOS is non-zero and nearly flat around this energy, what corresponds with the fact that gold is a good conductor. We can see

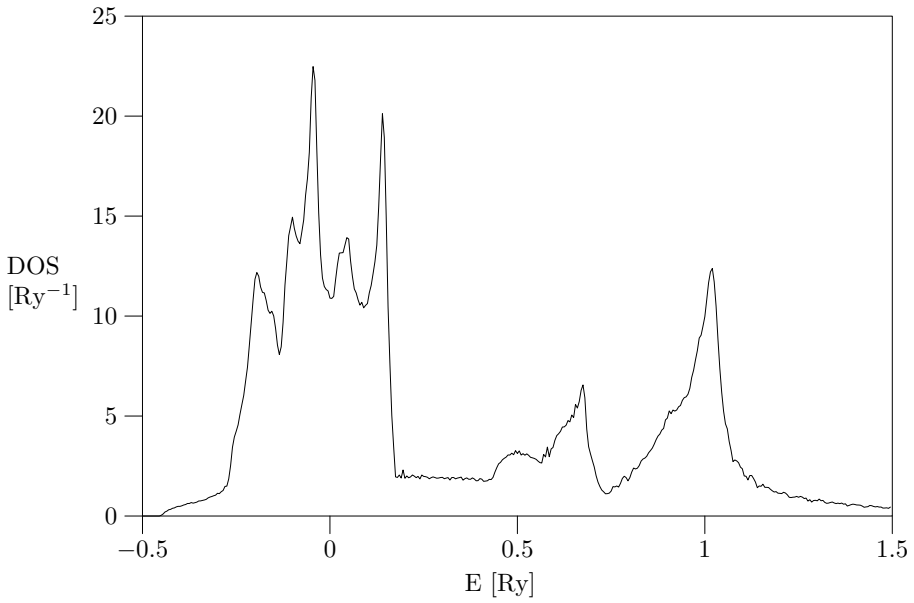

Figure 2.5: Density of states calculated from eigenvalues in **k**-space. Eigenvalues were evaluated in 64000 points in the **k**-space in a part that represents one quarter of the first Brillouin zone.

that the DOS is similar to the density of states of the clusters shown on the Fig. 2.3, the functions have peaks near energies $E = 0$ Ry and $E = 1$ Ry. However, there are differences that are probably mostly due to surface effects.

Chapter 3

Green's functions

Green's functions are useful for calculations of various properties of quantum systems. There are many variants that are suitable for various pourposes and are treated in standard books (Economou (1983), Fetter and Walecka (1971)). In our calculations we use the single particle time-independent Green's functions.

Green's function of the time-dependent Schrödinger equation allows us to find solution of the time-evolution with an arbitrary initial condition. Moreover, various measurable quantities can be expressed in terms of the Green's functions. Time-independent single particle Green's function $G(r, r', z)$ (resolvent), defined as

$$(z - H(r))G(r, r', z) = \delta(r - r')\,, \tag{3.1}$$

is Fourier transformation of the time-dependent function for case of time-independent Hamiltonian. The variable z is a complex variable that has a meaning of energy on the real axis.

3.1 Single electron Green's functions and self-energy

Retarded Green's function for non-interacting electrons is defined as

$$G^r(E) = (E + i\eta - H)^{-1}\,, \tag{3.2}$$

which in the spectral representation takes the form of

$$G^r(E) = \sum_k \frac{|k\rangle\langle k|}{E + i\eta - \epsilon_k}\,, \tag{3.3}$$

where $|k\rangle$ is a complete set of orthonormal eigenfunctions of the single particle Hamiltonian H with energy ϵ_k. As the Green's function has discontinuity on the real axis in the imaginary part, we need to add a small imaginary part η to the energy to pick either upper or lower solution. Adding positive η we calculate the retarded Green's function that determines the evolution of the system in time, while with negative η one gets the

advanced Green's function G^a that determines the evolution to the past. Furthermore we can define the spectral density $A(E) = i(G^r(E) - G^a(E))$ that gives the density of states.

The spectral representation of the retarded Green's function can be rewritten as

$$G^r(E) = \sum_k |k\rangle\langle k| \left[v.p. \left(\frac{1}{E - \epsilon_k} \right) - i\pi\delta(E - \epsilon_k) \right] , \tag{3.4}$$

where $v.p.$ denotes the principal value. From this equation if follows that the local density of states for orbital $|k\rangle$ can be calculated as

$$\varrho(k, E) = -\frac{1}{\pi} \Im\mathrm{m}(G^r_{k,k}(E)) , \tag{3.5}$$

where we use the matrix element of the retarded Green's function. The total density of states can be calculated as a sum of the local densities, being usually written as

$$\varrho(E) = -\frac{1}{\pi} \mathrm{Tr} \Im\mathrm{m}(G^r_{i,j}(E)) . \tag{3.6}$$

The distribution of the occupied states is in equilibrium given by the Fermi distribution, therefore we can calculate the number of electrons by integration of the density of states multiplied by the Fermi distribution.

In this paragraph we introduce the concept of self-energy on a single-electron level. It describes the effect of enlargement of the Hilbert space on the Green's function. The procedure is similar to the perturbation theory equations but we are able here to sum all the orders of the perturbation into a single term. We add to our Hamiltonian H_{11} a Hamiltonian H_{22} and interaction between them so that the total Hamiltonian reads

$$H = \begin{pmatrix} H_{11} & H_{12} \\ H_{21} & H_{22} \end{pmatrix} .$$

Now we want to find the change of the Green's function of the subspace 1 (our original part) after this addition. In other words, we want to invert the whole matrix $E - H$ and compare the element 11 with the inversion of $E - H_{11}$. We start from the eigenvalue equation

$$(EI - H)c = \begin{pmatrix} EI_{11} - H_{11} & -H_{12} \\ -H_{21} & EI_{22} - H_{22} \end{pmatrix} \begin{pmatrix} c_1 \\ c_2 \end{pmatrix} = \begin{pmatrix} 0 \\ 0 \end{pmatrix} ,$$

we substitute the solution of the equation for c_2 into the equation for c_1 yielding

$$(EI_{11} - H_{11} - H_{12}(EI_{22} - H_{22})^{-1} H_{21}) c_1 = 0 , \tag{3.7}$$

which is rewritten in terms of the Green's functions ($G^0_1 = (E - H_{11})^{-1}$) as

$$([G^0_1]^{-1} - H_{12} G^0_2 H_{21}) c_1 = 0 . \tag{3.8}$$

Comparison with the equation for the Green's function of the whole system gives

$$G_1 = \frac{1}{[G^0_1]^{-1} - \Sigma} , \tag{3.9}$$

where the self-energy is found to be

$$\Sigma = H_{12}(E - H_{22})^{-1}H_{21}\,. \tag{3.10}$$

When we calculate the retarded functions we add small imaginary part to the energy and the self energy can by divided into two parts: hermitian Δ and anti-hermitian $\frac{1}{2}\Gamma$. While the hermitian part shifts the energy levels, the anti-hermitian smears them.

3.2 Properties in a non-orthogonal basis set

In our calculations we use the matrix formulation of the Green's functions as was derived by Xue *et al.* (2002). The derivation of the transport equations can be found in various papers for various quantum approaches and we can refer to the standard book of Haug and Jauho (1996). The system can be divided into three parts: left and right electrodes and a central part (C). The right (R) and left (L) leads are taken to be sufficiently large and in equilibrium with chemical potentials μ_R and μ_L. At time $t = t_0$ the parts are connected and charge transport occurs. After some time is reached the steady state and when the $\mu_R \neq \mu_L$ the current can flow through the central part.

One difference that we need to take into account is that we use a non-orthogonal basis set with overlap matrix S. Because of this, we can represent the Green's function in the original basis and in the dual basis. Throughout this work we write $G(E)$ for Green's function matrix and $\mathfrak{g}$ for Green's function matrix in the dual basis (see Appendix A for more details concerning the non-orthogonal basis). Various aspects of the non-orthogonal basis are discussed by Artacho and del Bosch (1991), Priyadarshy *et al.* (1996) and Thygesen (2006). Equation 3.2 for the retarded Green's function matrix in the non-orthogonal basis reads

$$(E^+S - H)\mathfrak{g}^r = I\,, \tag{3.11}$$

where $E^+ = E + i\eta$.

Equation for the self-energy (Eq. 3.10) is modified in the non-orthogonal basis as

$$\Sigma^r_{L,ij} = (E^+S_{\mathrm{CL}} - H_{\mathrm{CL}})\mathfrak{g}^r_{\mathrm{L}}(E^+S_{\mathrm{LC}} - H_{\mathrm{LC}})\,, \tag{3.12}$$

where H_{LC} is the block of the total Hamiltonian between the left lead and the central part.

All the quantities are energy-dependent, we therefore need to input the bias V that is the device connected to into the equations. We can assume that the bias is divided evenly between the right and left lead – we put energy shifts $+V/2$ on the left lead and $-V/2$ on the right lead. In this case, the energy states in the left lead are shifted $V/2$ upwards and we need to use $\Sigma_L(E - V/2)$ and $\Sigma_R(E + V/2)$ to calculate the Green's function of the central part for energy E.

The retarded Green's function does not contain statistic distribution of the particles. For systems in equilibrium we can define the lesser Green's function as

$$\mathfrak{g}^<_{L,ij} = i(\mathfrak{g}^r_{L,ij} - \mathfrak{g}^a_{L,ij})f(E - \mu_L)\,, \tag{3.13}$$

where L is a sign for the left lead and $f(E)$ is the Fermi distribution. Similar equation holds for the right (R) lead. In the case of noninteracting electrons can this definition, in terms of single electron Green's function, be justified from full many-body description. In contrast to retarded and advanced functions it contains the information about the population of the single-electron levels both in equilibrium (eq. 3.13) and out of equilibrium (eq. 3.15) bellow (see book of Haug and Jauho (1996)).

For further calculation we define coupling as

$$\Gamma_{L,ij} = \mathrm{i}(\Sigma^r_{L,ij} - \Sigma^a_{L,ij})\,. \tag{3.14}$$

Using this we can calculate the lesser Green's function out of equilibrium in the central part with equation

$$\mathfrak{g}^<_{ij} = [\mathfrak{g}^r \Gamma_L \mathfrak{g}^a] f(E-\mu_L) + [\mathfrak{g}^r \Gamma_R \mathfrak{g}^a] f(E-\mu_R)\,. \tag{3.15}$$

The charge can be found by integration of the lesser Green's function over the energy as

$$Q = \frac{1}{2\pi}\int_{-\infty}^{\infty} \mathrm{d}E \mathrm{Tr}[\mathrm{S}\mathfrak{g}^<]\,. \tag{3.16}$$

The transmission function can be found (Haug and Jauho (1996)) as

$$T(E,V) = \mathrm{Tr}[\Gamma_L(E-V/2)\mathfrak{g}^r(E)\Gamma_R(E+V/2)\mathfrak{g}^a(E)] \tag{3.17}$$

and current by integration of the transmission as (with 2 for spin summation)

$$I(V) = \frac{2e}{h}\int \mathrm{d}E\, T(E,V)(f(E-V/2-\mu_L) - f(E+V/2-\mu_R))\,. \tag{3.18}$$

Diagonalization of the transmission function matrix divides the total conductance into contributions of different eigenchannels. These eigenchannels give information about the electronic states that contribute to the conductance. The eigenvalues of the transmission matrix – eigenchannel transmissions – give conductance of corresponding eigenchannels.

Following the theoretical results of previous works we could insert vibration into our model in the framework of the perturbation theory by introducing self-energies and Green's functions connected with the vibrational degrees of freedom. The calculation of transport properties with vibrations is discussed by Lake *et al.* (1997) on the case of semiconductors.

Chapter 4

Surface Green's function

When we place a cluster of atoms on the surface, the electronic states in the cluster change. How they change is determined by the interaction with the surface and the electronic properties of the surface. There are two effects: the electronic states are shifted, and the levels are smeared, which means that the levels have certain lifetime and the electrons are allowed to move in and out of the cluster. The actual size of these effects is given by the surface Green's function that we are going to calculate in this chapter.

4.1 Transformation of the Hamiltonian

As we showed in the last chapter, the transport properties can be calculated from the Hamiltonian. We consider a system similar to the one depicted on Fig 1.2. It is convenient to divide the system to the leads and the central part called also extended molecule which includes the molecule itself and the contacts.

The total Hamiltonian can be therefore written as

$$H = \begin{pmatrix} H_{\mathrm{L}} & H_{\mathrm{LC}} & 0 \\ H_{\mathrm{CL}} & H_{\mathrm{C}} & H_{\mathrm{CR}} \\ 0 & H_{\mathrm{RC}} & H_{\mathrm{R}} \end{pmatrix} \tag{4.1}$$

where C stands for the extended molecule, R and L for the leads. Here we assume that the overlap and interaction between the two leads can be neglected. The effect of the molecule is screened (Stokbro *et al.* (2005)) in a couple of atomic layers so there is almost no influence on the electronic states in the leads. In this case the leads serve as a source and drain of the incoming and outgoing electrons.

From the self-energy equation (3.10) it can be seen that we need only that part of the lead Green's function that has a non-zero interaction with the extended molecule. In other words, in our localized basis set, we need only the surface part of the lead Green's function.

In our calculations we consider the leads to be ideal semi-infinite gold electrodes. In this case the surface Green's function can be calculated with different methods (López

Sancho *et al.* (1984, 1985), for overview see Velev and Buttler (2004)). The main idea is to transform the basis atomic orbitals to 2D-Bloch functions in coordinates parallel to the surface $\mathbf{r}_\parallel$. Wave functions from l neighbouring layers are furthermore grouped to form a principal layer, having m orbitals per atom, the Bloch function for principal layer j reads

$$\Psi_j(\mathbf{k}_\parallel) = \begin{pmatrix} \psi_j^{11}(\mathbf{k}_\parallel) \\ \vdots \\ \psi_j^{\alpha\beta}(\mathbf{k}_\parallel) \\ \vdots \\ \psi_j^{lm}(\mathbf{k}_\parallel) \end{pmatrix},$$

where

$$\psi_j^{\alpha\beta}(\mathbf{k}_\parallel) = N^{-1/2} \sum_{\mathbf{r}_\parallel} \exp(\mathrm{i}\mathbf{k}_\parallel \cdot \mathbf{r}_\parallel) \varphi_j^{\alpha\beta}(\mathbf{r}_\parallel), \tag{4.2}$$

where α is an index for atomic planes and β indexes orbitals. By applying this transformation we diagonalize the Hamiltonian according to $\mathbf{k}_\parallel$, which can be schematically depicted as

$$H_\mathrm{L} = \begin{pmatrix} h_{11} & h_{12} & h_{13} & \dots \\ h_{21} & h_{22} & h_{23} & \dots \\ h_{31} & h_{32} & h_{33} & \dots \\ \vdots & \vdots & \vdots & \ddots \end{pmatrix} \Longrightarrow H_\mathrm{L} = \begin{pmatrix} h(\mathbf{k}_1) & 0 & 0 & \dots \\ 0 & h(\mathbf{k}_2) & 0 & \dots \\ 0 & 0 & h(\mathbf{k}_3) & \dots \\ \vdots & \vdots & \vdots & \ddots \end{pmatrix}$$

where $h(\mathbf{k}_n)$ are semi-infinite. The elements are calculated with equations similar to the equations 2.14 and 2.15. Moreover, the Hamiltonian for each $\mathbf{k}_{||}$ has a block-diagonal form because each principal layer interacts only with the two nearest principal layers. So we can separate the Hamiltonian in parts for each $\mathbf{k}_\parallel$

$$h(\mathbf{k}_n) = \begin{pmatrix} H_{00} & H_{01} & 0 & \dots \\ H_{10} & H_{11} & H_{12} & \dots \\ 0 & H_{21} & H_{22} & \dots \\ \vdots & \vdots & \vdots & \ddots \end{pmatrix},$$

where each row and column represents one principal layer and the elements $H_{ij} = \langle \Psi_i | H | \Psi_j \rangle$.

4.2 Iterative method

The iterative method is based on the Hamiltonian partitioning technique presented in chapter 3 for orthogonal basis. However, the formula for self-energy is slightly different because we use a non-orthogonal basis set. The derivation can be repeated in a similar manner: from the Green's matrix equation

$$\begin{pmatrix} ES_{00} - H_{00} & ES_{01} - H_{01} \\ ES_{10} - H_{10} & ES_{11} - H_{11} \end{pmatrix} \begin{pmatrix} \mathfrak{g}_{00} & \mathfrak{g}_{01} \\ \mathfrak{g}_{10} & \mathfrak{g}_{11} \end{pmatrix} = \begin{pmatrix} 1 & 0 \\ 0 & 1 \end{pmatrix}$$

we have

$$\mathfrak{g}_{00} = [ES_{00} - H_{00} - (ES_{01} - H_{01})(ES_{11} - H_{11})^{-1}(ES_{10} - H_{10})]^{-1}\,, \tag{4.3}$$

where we can identify the self-energy

$$\Sigma = (ES_{01} - H_{01})(ES_{11} - H_{11})^{-1}(ES_{10} - H_{10})\,. \tag{4.4}$$

The procedure for calculation of the surface Green's function proceeds as follows: we start with Hamiltonian with $n+1$ principal layers. In each step we divide the Hamiltonian into two parts: the last principal layer and the rest. We calculate the Green's function of the last principal layer and then the self-energy contribution to the Hamiltonian of the rest using equation 4.4. Now we can repeat the procedure for Hamiltonian with n principal layers but with the self-energy.

This calculation is iterated until the Green's function converges. For the converged Green's matrix we have

$$\mathfrak{g}_{00} = [ES_{00} - H_{00} - (ES_{01} - H_{01})\mathfrak{g}_{00}(ES_{10} - H_{10})]^{-1}\,. \tag{4.5}$$

Since we are calculating retarded Green's function we add small $+i\eta$ to the energy. The convergence of this method is slow, the Green's function converges as $O(N^{-1})$, but this is the only method to use when dealing with different layers.

4.3 Accelerated iteration method

The drawback of the iterative method explained in the previous section is its slow convergence – each step only one principal layer is added. The convergence of method of López Sancho *et al.* (1985) is much faster, each step doubles the number of used principal layers, so instead of e.g. 2^8 iterations only 8 steps are needed. The original method was developed for orthogonal basis and since we use a non-orthogonal basis, the method has to be slightly modified.

We start with the matrix equation for Green's matrix in a basis of 2-D Bloch states $(ES - H)\mathfrak{g}(E) = I$. Because each principal layer interacts only with its nearest neighbours we get a system of equations for each $\mathbf{k}_\parallel$

$$\begin{pmatrix} ES_{00} - H_{00} & ES_{01} - H_{01} & 0 & \dots \\ ES_{10} - H_{10} & ES_{11} - H_{11} & ES_{12} - H_{12} & \dots \\ 0 & ES_{21} - H_{21} & ES_{22} - H_{22} & \dots \\ \vdots & \vdots & \vdots & \ddots \end{pmatrix} \begin{pmatrix} \mathfrak{g}_{00} & \mathfrak{g}_{01} & \dots \\ \mathfrak{g}_{10} & \mathfrak{g}_{11} & \dots \\ \mathfrak{g}_{20} & \mathfrak{g}_{21} & \dots \\ \vdots & \vdots & \ddots \end{pmatrix} = \begin{pmatrix} 1 & 0 & \dots \\ 0 & 1 & \dots \\ 0 & 0 & \dots \\ \vdots & \vdots & \ddots \end{pmatrix}$$

where

$$H_{ij} = \langle \Psi_i | H | \Psi_j \rangle\,, \tag{4.6}$$

S_{ij} are matrix elements between layers i and j and $\mathfrak{g}_{ij}$ are matrix elements between layers i and j in dual basis. The effect of the surface vanishes in our model for a layer that is

few layers beneath the surface. Therefore, the Hamiltonian blocks between layers in the crystal are the same. Moreover, we assume that also the blocks on and near the surface have the same elements: $H_{00} = H_{1\,1} = H_{n\,n}$ and $H_{1\,0} = H_{2\,1}$. This is not true completely because the atoms on a clean surface have lower density parameter. However, as we intend to place some cluster of atoms on the surface we can use this assumption. Therefore we have

$$\begin{aligned}
(ES_{00} - H_{00})\mathfrak{g}_{00} &= I + (H_{01} - ES_{01})\mathfrak{g}_{10} \\
(ES_{00} - H_{00})\mathfrak{g}_{nk} &= (H_{10} - ES_{10})\mathfrak{g}_{n-1\,k} + (H_{01} - ES_{01})\mathfrak{g}_{n+1\,k} \\
(ES_{00} - H_{00})\mathfrak{g}_{nn} &= I + (H_{10} - ES_{10})\mathfrak{g}_{n-1\,n} + (H_{01} - ES_{01})\mathfrak{g}_{n+1\,n}
\end{aligned} \tag{4.7}$$

where the last two equations hold $\forall n > 1$.

Now we introduce a notation

$$\varepsilon^0 = \varepsilon_s^0 = H_{00}\,, \quad \alpha^0 = (H_{01} - ES_{01})\,, \quad \beta^0 = (H_{10} - ES_{10})\,. \tag{4.8}$$

With this the eqs. 4.7 are rewritten as

$$(ES_{00} - \varepsilon_s^0)\mathfrak{g}_{00} = I + \alpha^0\mathfrak{g}_{10} \tag{4.9}$$

$$(ES_{00} - \varepsilon^0)\mathfrak{g}_{nk} = \beta^0\mathfrak{g}_{n-1\,k} + \alpha^0\mathfrak{g}_{n+1\,k} \tag{4.10}$$

$$(ES_{00} - \varepsilon^0)\mathfrak{g}_{nn} = I + \beta^0\mathfrak{g}_{n-1\,n} + \alpha^0\mathfrak{g}_{n+1\,n}\,. \tag{4.11}$$

Now we can insert eq. 4.10 for arbitrary k into eqs. 4.9 and 4.11 yielding

$$(ES_{00} - \varepsilon_s^0)\mathfrak{g}_{00} = I + \alpha^0(ES_{00} - \varepsilon^0)^{-1}[\alpha^0\mathfrak{g}_{2\,0} + \beta^0\mathfrak{g}_{0\,0}] \tag{4.12}$$

$$\begin{aligned}
(ES_{00} - \varepsilon^0)\mathfrak{g}_{nn} = I &+ \alpha^0(ES_{00} - \varepsilon^0)^{-1}[\alpha^0\mathfrak{g}_{n+2\,n} + \beta^0\mathfrak{g}_{n\,n}] + \\
&+ \beta^0(ES_{00} - \varepsilon^0)^{-1}[\alpha^0\mathfrak{g}_{n\,n} + \beta^0\mathfrak{g}_{n-2\,n}]\,.
\end{aligned} \tag{4.13}$$

And

$$(ES_{00} - \varepsilon_s^0 - \alpha^0(ES_{00} - \varepsilon^0)^{-1}\beta^0)\mathfrak{g}_{00} = I + \alpha^0(ES_{00} - \varepsilon^0)^{-1}\alpha^0\mathfrak{g}_{2\,0} \tag{4.14}$$

$$\begin{aligned}
(ES_{00} - \varepsilon^0 - \alpha^0(ES_{00} - \varepsilon^0)^{-1}\beta^0 - \beta^0(ES_{00} - \varepsilon^0)^{-1}\alpha^0)\mathfrak{g}_{nn} = I + \\
+\alpha^0(ES_{00} - \varepsilon^0)^{-1}\alpha^0\mathfrak{g}_{n+2\,n} + \beta^0(ES_{00} - \varepsilon^0)^{-1}\beta^0\mathfrak{g}_{n-2\,n}\,.
\end{aligned} \tag{4.15}$$

Now we use

$$\varepsilon^1 = \varepsilon^0 + \alpha^0(ES_{00} - \varepsilon^0)^{-1}\beta^0 + \beta^0(ES_{00} - \varepsilon^0)^{-1}\alpha^0\,, \tag{4.16}$$

$$\varepsilon_s^1 = \varepsilon^0 + \alpha^0(ES_{00} - \varepsilon^0)^{-1}\beta^0\,, \tag{4.17}$$

$$\alpha^1 = \alpha^0(ES_{00} - \varepsilon^0)^{-1}\alpha^0 \tag{4.18}$$

$$\beta^1 = \beta^0(ES_{00} - \varepsilon^0)^{-1}\beta^0\,. \tag{4.19}$$

With this the eqs. 4.9–4.11 can be rewritten as

$$(ES_{00} - \varepsilon_s^1)\mathfrak{g}_{00} = I + \alpha^1\mathfrak{g}_{2\,0} \tag{4.20}$$

$$(ES_{00} - \varepsilon^1)\mathfrak{g}_{nk} = \beta^1\mathfrak{g}_{n-2\,k} + \alpha^1\mathfrak{g}_{n+2\,k} \tag{4.21}$$

$$(ES_{00} - \varepsilon^1)\mathfrak{g}_{nn} = I + \beta^1\mathfrak{g}_{n-2\,n} + \alpha^1\mathfrak{g}_{n+2\,n}\,. \tag{4.22}$$

These equations are equivalent to eqs. 4.9–4.11 but we have Green's function elements between even layers only. The whole procedure can be repeated from the beginning until matrices α^i and β^i are small.

After a sufficient number of iterations the equations 4.20 and 4.22 are

$$(ES_{00} - \varepsilon_s^i)\mathfrak{g}_{00} = I \tag{4.23}$$

$$(ES_{00} - \varepsilon^i)\mathfrak{g}_{nn} = I \tag{4.24}$$

and we can calculate the surface and bulk Green's functions (for appropriate $\mathbf{k}_\parallel$)

$$\mathfrak{g}_{00} = (ES_{00} - \varepsilon_s^i)^{-1} \tag{4.25}$$

$$\mathfrak{g}_{nn} = (ES_{00} - \varepsilon^i)^{-1} \tag{4.26}$$

4.4 Transformation to coordinate space

We implemented both mentioned methods and verified that they give the same results. For further calculations we used the latter method that is faster.

From the calculation we get the Green's matrix in dual basis in point $\mathrm{k}_\parallel$. For further calculation we need to make a transformation from the $\mathbf{k}_\parallel$-space to the $\mathbf{r}$-space. The basis transformation is (we omit the indices)

$$|\psi(\mathbf{r})\rangle = N^{-1/2} \sum_{\mathbf{k}_\parallel} \exp(-\mathrm{i}\,\mathbf{k}_\parallel \cdot \mathbf{r}_\parallel)|\varphi(\mathbf{k})\rangle\,, \tag{4.27}$$

where the summation is over points in the first Brillouin zone in the $\mathbf{k}_\parallel$ space.

The matrix element of the Green's function in the coordinate space can be calculated as

$$G(\mathbf{r}'_\parallel, \mathbf{r}_\parallel) = \langle\psi_{\mathbf{r}'_\parallel}|G|\psi_{\mathbf{r}_\parallel}\rangle = N^{-1} \sum_{\mathbf{k}_\parallel} \sum_{\mathbf{k}_\parallel{}'} \exp(\mathrm{i}\,\mathbf{k}'_\parallel \cdot \mathbf{r}'_\parallel)\langle\varphi_{\mathbf{k}'_\parallel}|G|\varphi_{\mathbf{k}_\parallel}\rangle \exp(-\mathrm{i}\,\mathbf{k}_\parallel \cdot \mathbf{r}_\parallel) =$$

$$= N^{-1} \sum_{\mathbf{k}_\parallel} \exp(\mathrm{i}\,\mathbf{k}'_\parallel \cdot (\mathbf{r}'_\parallel - \mathbf{r}_\parallel))G(\mathbf{k}_\parallel)\,. \tag{4.28}$$

For diagonal block ($\mathbf{r}_\parallel = \mathbf{r}'_\parallel$) the last equation yields a simple relation

$$G(\mathbf{r}_\parallel, \mathbf{r}_\parallel) = N^{-1} \sum_{\mathbf{k}_\parallel} G(\mathbf{k}_\parallel)\,. \tag{4.29}$$

As the problem is laterally invariant, the Green's function does depend only on the difference $\mathbf{r}'_\parallel - \mathbf{r}_\parallel$.

One must note that the procedures in previous sections give Green's function matrix in dual basis, whereas eq. 4.28 holds for matrix elements. Therefore we have to transform the calculated matrix $\mathfrak{g}(\mathbf{k}_\parallel)$ to $G(\mathbf{k}_\parallel)$ in each point of the $\mathbf{k}_\parallel$ space with the overlap matrix. This is the inverse transformation to transformation to the dual space.

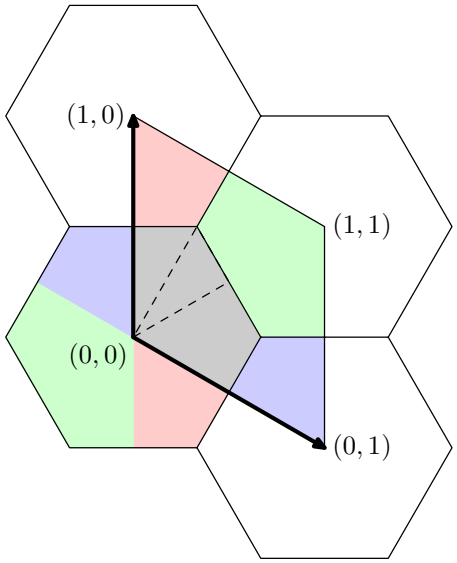

Figure 4.1: Transformation of the first Brillouin zone. The first BZ is the hexagonal shape area around the origin in the reciprocal space. The hexagonal shape resembles the density of states on the Fig 4.2. The zone was divided into four parts and three of the parts were shifted to equivalent positions. The final shape is a diamond, which is easier to parametrize. The backward transformation was effected over the points in the transformed area. Example of the first irreducible Brillouin zone is surrounded by the dashed line.

4.5 Implementation

The transformation from the $\mathbf{k}$-space to the coordinate space was done on a grid in the $\mathbf{k}_{\|}$-space spanning part equivalent to the first Brillouin zone as is shown in Fig 4.1. We used 160 intervals to divide each reciprocal vector and calculated the $\mathfrak{g}(\mathbf{k}_{\|})$ in a cycle over the points of the grid. Different way would be to calculate the $\mathfrak{g}(\mathbf{k}_{\|})$ only in the first irreducible zone and then transform it according to symmetry to get the matrix in symmetric points (the symmetry is figured in Fig. 4.2). However, this was not implemented but we used the symmetry of the reciprocal space to calculate the density of states of the bulk (Fig. 4.3). In this calculation we calculated the density of states in each point of a grid in the first Ir BZ and multiplied it with a multiplicity factor. This factor gives the number of different points that can be obtained from the original point with the symmetry operations of the point group of the reciprocal space. For most of the points it equals to 12 (in our case) but, for instance, it is equal to 1 for the origin.

To calculate matrix elements between atoms in one layer we use equation 4.28 with $G(\mathbf{k}_{\|})$ of the appropriate layer. To calculate matrix elements between two different layers we must use the $G(\mathbf{k}_{\|})$ matrix between these two layers. We calculated elements for 18 neighbours in the same plane and 12 neighbours in nearest neighbour plane. As follows from the symmetry, the matrices are not unique. There are three distinct matrices for

both the same plane and the nearest plane, all the other matrices can be calculated by transformation of these matrices.

We calculated the Green's function for Au (111) surface. To calculate other FCC (111) surfaces we would only need to change the parameters of the tight-binding model and the lattice constant. Calculation of other surfaces or other elementary cells would require a change of interplanar shifts, what can be done with little effort (we tested this for Au(100) surface).

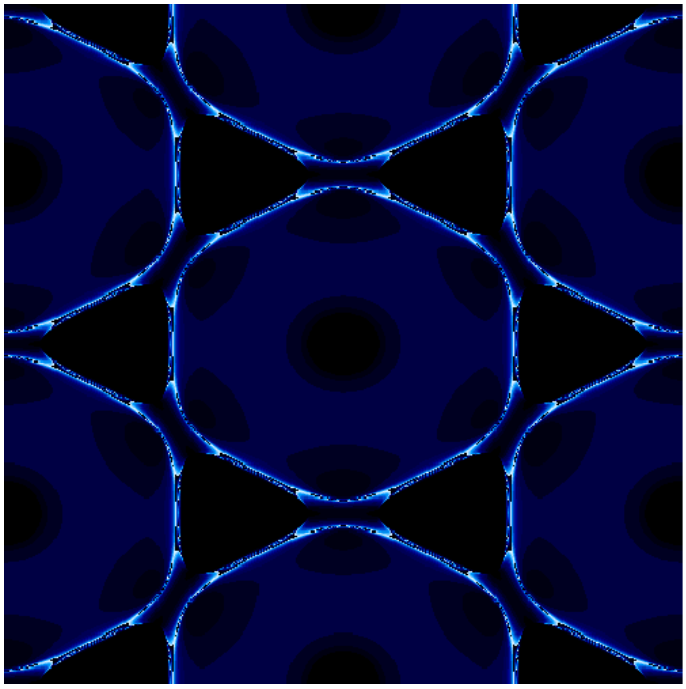

Figure 4.2: Bulk density of s-states in the $\mathbf{k}$-space obtained with the Green's function method. The energy was $E = 0.285 + 0.001\mathrm{i}\,\mathrm{Ry}$. Number of iteration steps differed in each point. As we want to illustrate the symmetry of the density of states we do not include the exact scale. Low density of states is represented with a dark color and high density are white.

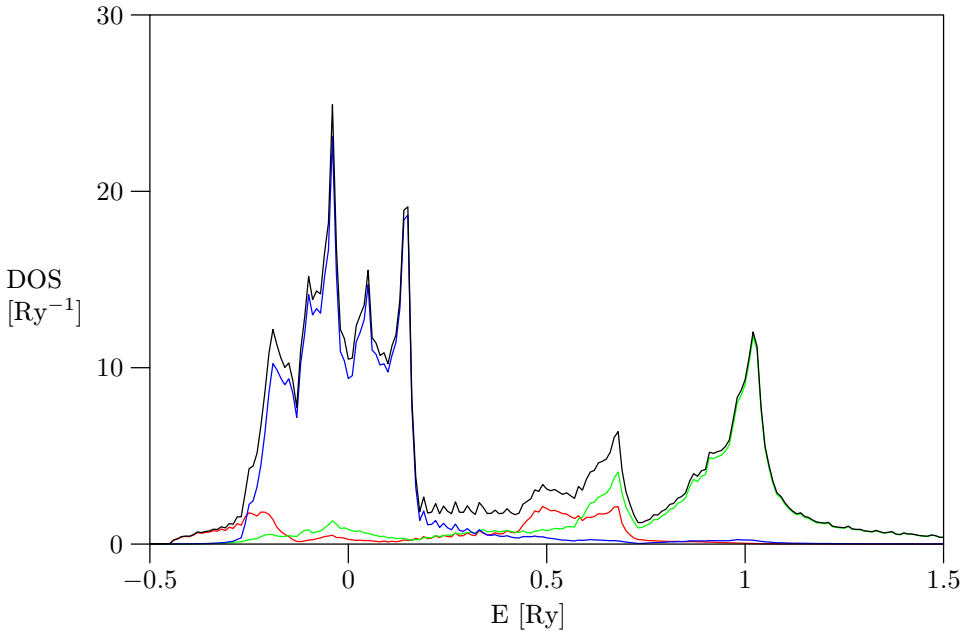

Figure 4.3: Bulk density of states obtained with the Green's function method. Imaginary part of the energy was $\eta = 0.001$Ry. One principal layer was made up by three layers. Green's function was calculated in each point of a grid in the first Ir BZ and multiplied by appropriate overlap matrix. The DOS is not so smooth compared to the Fig. 2.5 becuse a lower number of points was used.

Chapter 5

Density of states in tip

Measurements of the current-voltage dependencies done with single molecules or atomic wires usually do not control the exact geometry of the metal contacts where the molecule is placed. Among other things we want to know, at last qualitatively, if the transport properties are affected for different shapes of the tip and how this is relater to the density of states of the tip or contact. Another interesting thing is a comparison between our method and the wide-band limit that supposes constant densities of states in the leads and is widely used in calculations, especially of inelastic transport properties.

5.1 Interaction of the tip with the surface

It is difficult to consider an arbitrary geometry of the contact. We will therefore restrict our work to the semiinfinite surface with a rather small cluster of atoms (called the tip in the text bellow) placed on it. We insert the effect of the surface on the tip with the self-energy. To find the matrix elements of Hamiltonian and overlap matrix between the surface and the tip the following procedure is used. Firstly we generate coordinates of the tip atoms using a simple program, in which we assume that the tip has a layered structure. Another two layers are added to represent the surface – they have the same atomic positions as the surface. We repeat the calculation for several tip geometries. (We use two layers to represent the surface because the tip does not interact with more layers in the crystal.) For each tip we calculate the Hamiltonian and overlap matrices. Then we can calculate the self-energy of the crystal using blocks of the Hamiltonian and overlap matrices between the last two layers and the tip using the equation 3.12. The tip Green's function in the presence of the surface is then

$$\mathfrak{g}_T = [(ES - H)_T - (ES - H)_{TL}\mathfrak{g}_L(ES - H)_{LT}]^{-1}\,, \tag{5.1}$$

where the T (L) is index for tip (lead).

As we stated in the previous chapter, we need to transform the matrix elements of the surface Green's function G to matrix elements in the dual basis $\mathfrak{g}$. We use a separate procedure to perform this transformation. According to the transformation A.12, we have

to multiply G with inversion of the overlap matrix of the crystal from both sides. To avoid calculation of the inverse matrix of the whole crystal we replace the surface with sufficiently large cluster of atoms with three surface layers and we calculate appropriate G for these three layers (up to 3$^{\text{rd}}$ nearest neighbours in layer and in the nearest layer). The inversion of the overlap matrix is calculated and used to transform the G to $\mathfrak{g}$. In our calculations we need only the elements of the first and second layer, they are taken as matrix elements between atom in the centre of the first or second layer and appropriate atoms around it. We verified that the number of atoms we used in the cluster was sufficient and that the procedure did not suffer from numerical errors (e.g. from the calculation of the matrix inversion). However, we got some unphysical behaviour when we use the Green's function matrices for first neighbours, therefore we had to use only diagonal (on-site) blocks of the Green's matrix in all the following calculations.

The procedure for evaluation of the density parameters ρ_i has to be modified to calculate these parameters properly. We cannot use only a loop over all atoms as we did in previous calculations because we would not include some of the atoms in the crystal that would have non-zero contribution (coordinates of some atoms of the surface are stored to calculate the interaction part of the Hamiltonian). We divided the calculation to solve this problem like this: the density on atom i is a sum over all non-surface tip atoms (the tip itself) plus density on layer

$$\rho_i = \sum_{j \in \text{tip}} \rho_{ij} + \rho_{\text{layer}} \,, \tag{5.2}$$

where we get the ρ_{layer} in a separate calculation as a density for a single atom in the first and second layer away from a sufficiently large cluster of atoms that represents the surface. For the next layers the influence of the crystal vanishes and only tip atoms need to be considered in the calculation of the density parameter.

The density of states ϱ can be calculated using equation

$$\varrho = -\frac{1}{\pi} \Im m[Tr(\mathfrak{g}S)] \,, \tag{5.3}$$

where we have to use the overlap S matrix to obtain proper result. This equation gives density of states normalized to number of orbitals. The local density of states (LDOS) on particular atom (orbital) can be calculated with trace restricted to that atom (orbital). We use this value – the LDOS normalized to number of orbitals – in the figures.

5.2 Results

In our calculations we considered tips with different geometries, usually a tetrahedron cluster of various size was placed on the surface. To test another shape we also tried to add some more atoms close to the basic tetrahedron. For all of them we calculated the local density of states on the apex atom as this is one of the properties that influence the electron transport.

Figure 5.1: Examples of two tips used in calculations: tip 3-2-1 on the left side and tip 4-3-1 on the right side. The latter has one more line of atoms in first and second layer. Densities of states on the apex atoms of both tips are compared in Fig 5.6. Surface is not shown in this picture.

To understand various shapes of the tips we introduce our notation. The tip is formed by a set of layers (continuing the (111) side of the crystal). In each layer atoms form a triangle and the tip can be referred with a set of numbers giving a number of atoms in one side (or number of rows of the atoms) of the triangle in each layer. For example, 3-2-1 (Fig. 5.1, left) tip has three layers with three rows in the base layer (6 atoms), two rows in the second layer (3 atoms) and one atom in the third layer. In total, it has 10 atoms.

5.2.1 Self energies

From the equation 5.1 it follows that $\mathfrak{g}_T$ is computed from the Green's function of the noninteracting tip and the self-energy of the surface – effect of the surface on the tip. One of the approaches to include the latter complicated term is the wide-band approximation (WBL). In this approximation we replace the surface density of states with a constant. The surface Green's function can be therefore replaced with a diagonal imaginary matrix. The diagonal elements have to be negative to represent the retarded function. The self-energy can then be calculated as usual.

Fig. 5.2 shows the local density of states on the apex atom of a four-atom tip connected to the surface with constant density of states. The data were computed for $\mathfrak{g}_L = -iI$, where I is the identity matrix. Red line in the graph represents local density of states calculated with the energy dependent Green's function. The plot also shows all the eigenvalues of a tip that is placed on the surface but does not interact with it. In this case only the density parameter (see equation 5.2) is influenced by the surface. Analysis of the eigenvalues shows that the peak near the Fermi energy comes from the s-state on the apex atom of the tip that is important for the transport. The peak (smeared in the WBL) to the right from the Fermi energy comes from the p_z state (perpendicular to the surface) of the apex atom.

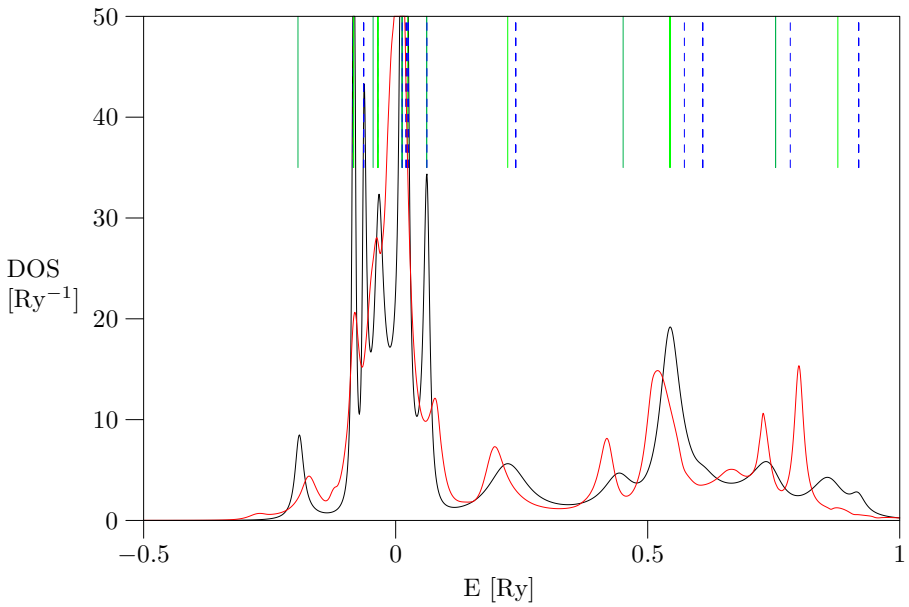

Figure 5.2: Local density of states on apex atom of the four-atom 2-1 tip (black line) in the wide-band limit and with energy dependent surface Green's function (red line). Eigenvalues of Hamiltonian of four-atom tip that is placed on the surface but does not interact with it (blue dashed lines, eigenvalues with the highest projection of their eigenvector to the apex orbitals (green lines) and with second highest projection (dark green lines)). The shape of the tip is tetrahedron with three base atoms and one apex atom.

5.2.2 One atom on surface

The effect of replacement of the exact self-energy calculated using the method of the previous chapter with the wide-band limit can be shown on the density of states of one gold atom on the Au (111) surface. In Fig. 5.3 are the initial states of a single atom on surface but without interaction with the surface and the density of states after the addition of the surface self-energy. Two lines represent total density of states in the wide-band limit (black) and with the tight-binding self-energy (red). For the wide-band approximation, the surface Green's function was replaced by diagonal matrix with diagonal elements equal to $-c\mathrm{i}$, the presented DOS is calculated for $c = 1$.

The figure illustrates the effect of the WBL and realistic Green's function on the LDOS. The density of states in the WBL is just sum of Lorentzian functions that replaced the δ functions in the eigenvalues of the Hamiltonian. In contrast, density of states calculated with the tight-binding self-energy shows finer structure: for example, the p-states peak near $E = 0.6$ Ry shifts to lower energy and has bumps on both sides. Also the s-density extents more to lower energies adding to the plateau around -0.2 Ry. In both calculations is formed a plateau around the Fermi energy.

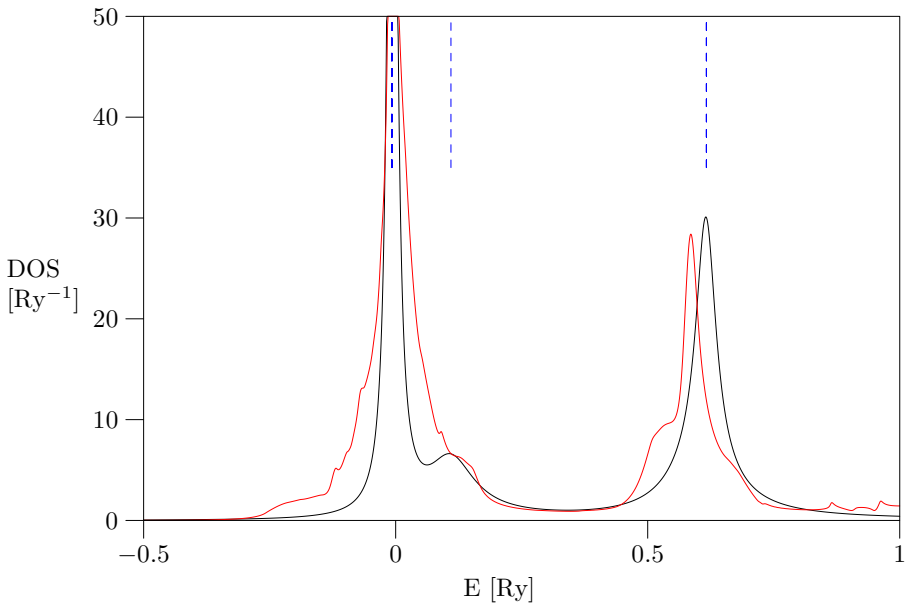

Figure 5.3: One atom on the surface. Density of states (black) of atom on the surface in the wide-band approximation, atomic levels without addition of the self-energy (vertical lines) and local density of states with diagonal blocks of Au (111) surface Green's function (red).

5.2.3 Shape effects

Here we are interested in the dependence of the local density of states on a tip shape. We will consider tips of tetrahedron shape and tips with additional atoms added to this basic shape.

In all cases the density of states has a shape that is similar to the one shown in Fig. 5.4: d-states form a structured peak in the interval around zero energy of the model, s-states occupy energies around the Fermi energy $E_F = 0.285$ Ry and the p-states are responsible for the structures in the higher energies. The density is similar to the density of states of the bulk (Figs 2.5 and 4.3) but it shows finer structure than the bulk density. Similarly to the 2-1 tip, the eigenvalue analysis shows the peak near the Fermi energy comes from s-state of the apex atom. The LDOS for both surface Green's functions are similar but we can see that s and p peaks also show shift to lower energies for the tight-binding self energy.

We compared LDOS an apex atoms for symmetric tetrahedron tips with a different number of layers, as an example, the local densities of states for three tips: 2-1, 3-2-1 and 4-3-2-1 are shown in Fig. 5.5. As the number of layers grows, small peaks in the LDOS shift towards the Fermi energy and fill the energy interval around it.

We also calculated densities of states for tips that are not symmetric but have more atoms on their sides (like the tip in Fig. 5.1, right). As an example, figure 5.6 shows local

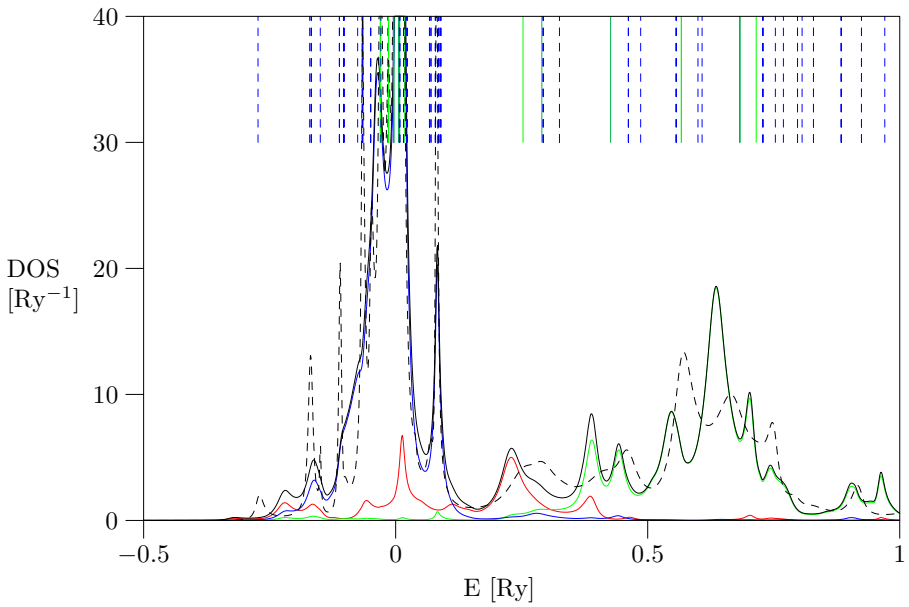

Figure 5.4: Density of states on the apex atom of pyramidal 3-2-1 tip with 10 atoms (three layers with 6 (base), 3 and 1 (apex) atom). Shown are local densities of states projected to the s (red), p (green) and d (blue) orbitals and the total local density on the apex atom (black). Diagonal blocks of the surface Green's function were used. Black dashed line represent density of states in for constant self-energy (WBL). Vertical lines mark eigenvalues of the tip that is placed on the surface but does not interact with it. Eigenvalues with the highest eigenvector projection on one of the nine orbitals on the apex atom are drawn with green line, eigenvalues with second highest projection are drawn with dark green line, the rest of the eigenvalues is signed with dashed blue line.

densities of states on the apex atom for 3-2-1 and 4-3-1 tip. One can see that the presence of other atoms near the apex atom lowers the peaks or splits them resulting in a function that is flatter. Similar characteristic (flattening) can be also find for the apex atom LDOS of tips with higher number of layers. We compared DOS for tips up to seven layers and number of atoms in the tip up to 53.

As we can see from the transport equation the local densities of states on the apex atom have an important effect on the transport. The local density enters the equation in the Γ factor (see 3.17). Moreover, the factor is in the equation squared so that the zero-bias conductance depends significantly on the tip apex LDOS at the Fermi energy. The calculations give similar densities at the Fermi energy for different tips but very different for other energies. We can argue that the shape of the LDOS can shift or change after we connect the tip to the molecule. The self-consistent procedure (next section) also shifts the levels and similarly we can get different LDOS from *ab initio* calculations. The LDOS of different tips differs, for example, for energies near 0.2 Ry in Fig. 5.5: the LDOS of the 2-1 tip has a peak whereas the LDOS for the 4-3-2-1 tip is roughly ten times lower. If this

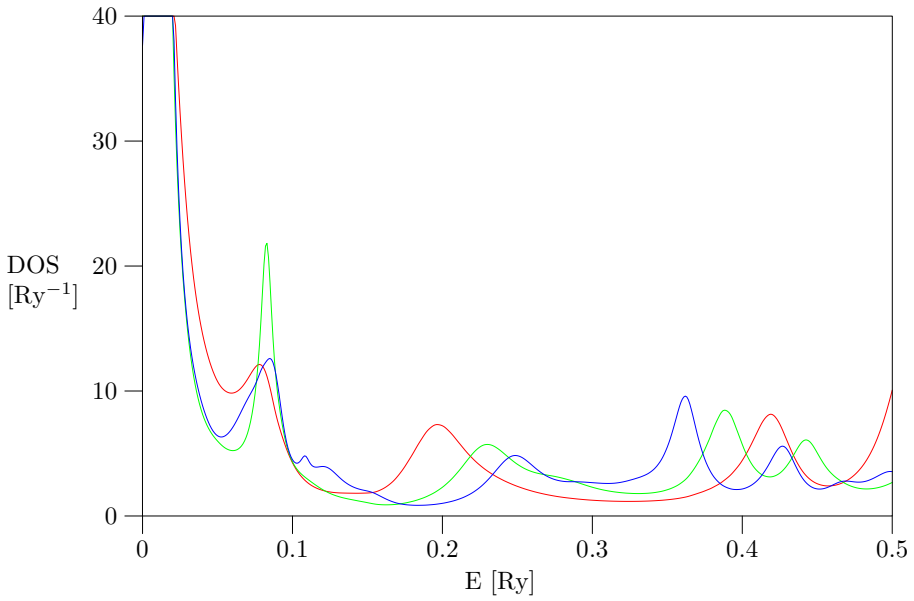

Figure 5.5: Local density of states on the apex atom for pyramidal tips with different size. Tip of type 2-1 with 4 atoms (red line), type 3-2-1 with 10 atoms (green line) and 4-3-2-1 tip containing 20 atoms (blue line). Interval around the Fermi energy $E_F = 0.285$ Ry is shown. Diagonal blocks of the surface Green's function were used.

situation was at the Fermi energy the zero-bias conductance could differ by two orders. We can conclude that the LDOS can differ significantly for different sharp tetrahedron tips. The LDOS for tips with wider base is more smeared but still the difference can result in an one order difference in the zero-bias conductance.

5.2.4 Self-consistent calculation

The charge self-consistent iterative procedure (section 2.2.1) was implemented. In each step of the iteration the number of electrons for each atom of the tip was calculated from the retarded Green's function and the on-site potential shifts were changed according to the charge of the atom. In this calculation there were little or no problems with the convergence of the local potential shifts.

In Fig. 5.7 are local densities of states on the apex atom of 4-3-2-1 tip before and after the self-consistent procedure. The potential shift for the apex atom was $\phi = 0.09\,\mathrm{Ry}$ what coincides with the value of the shift of the peaks in the plot. The potential shifts ϕ_i depend significantly on the position of the atom i in the tip. The value is low for base and central atoms and is higher for atoms on the surface of the tip. Because of this, the densities are not just shifted on the energy axis but they have slightly different shape.

The lower importance of this procedure for atoms surrounded by other atoms can by illustrated on a case of a single layer tip with a shape of a diamond with one side containing

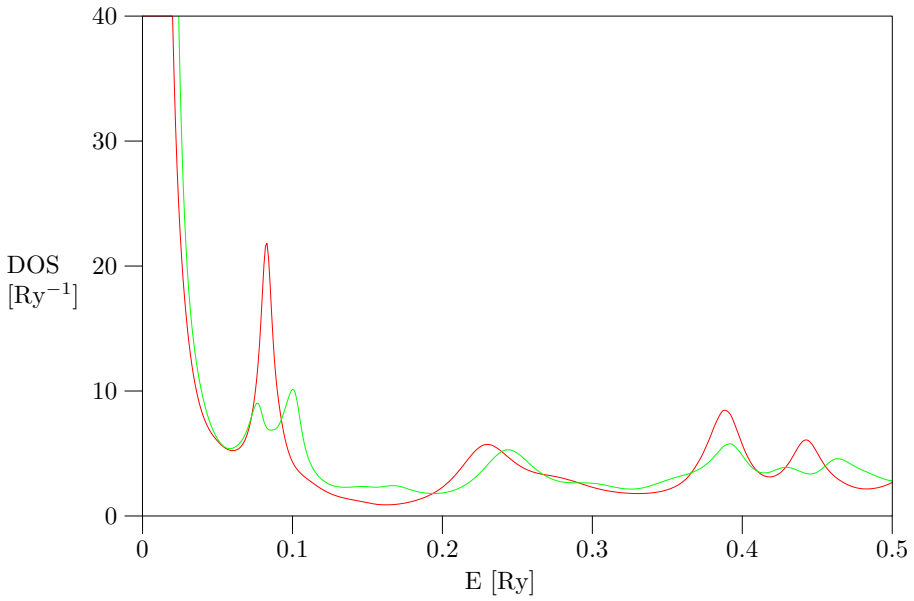

Figure 5.6: Local density of states for two tips with different shape. First is 3-2-1 tip with 10 atoms in three layers (6 (base), 3, 1 (apex)) (red line). Second is 4-3-1 tip with three layers containing 10 atoms in the base layer, 6 in the second layer and one apex atom. The presence of other atoms in the vicinity of the apex atom seems to flatten the density of states for the bigger tip.

5 atoms, in other words 5 rows each with 5 atoms, 25 atoms in total. Figure 5.8 shows the local density of states of atom in the center of the single layer tip. The potential shift on this atom was only $\phi = 0.01\,\mathrm{Ry}$ and the densities are very similar.

From the calculations it seems that the electronic properties of atoms lacking their neighbours are not described properly in the model and large potential shifts have to be applied for these atoms. The apex atom of the tip 4-3-2-1 has only three of his eight possible first neighbours whereas the central atom of the single layer tip lacks three of them. The peak in the density of states for 4-3-2-1 tip near the Fermi energy has shifted nearer to the Fermi energy increasing the LDOS at this energy from $2.7\,\mathrm{Ry}^{-1}$ to $3.9\,\mathrm{Ry}^{-1}$. We must remember that these potential shifts in this case have no physical meaning and are only a way of improving the calculations.

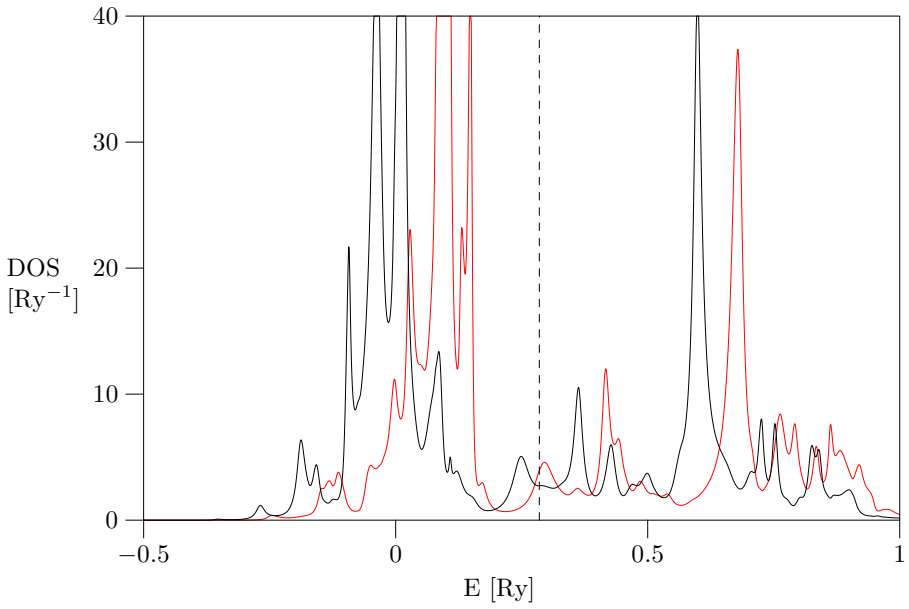

Figure 5.7: Density of states on the apex atom of 4-3-2-1 tip with 20 atoms before (black line) and after (red line) the self-consistent procedure. Dashed vertical line marks the Fermi energy.

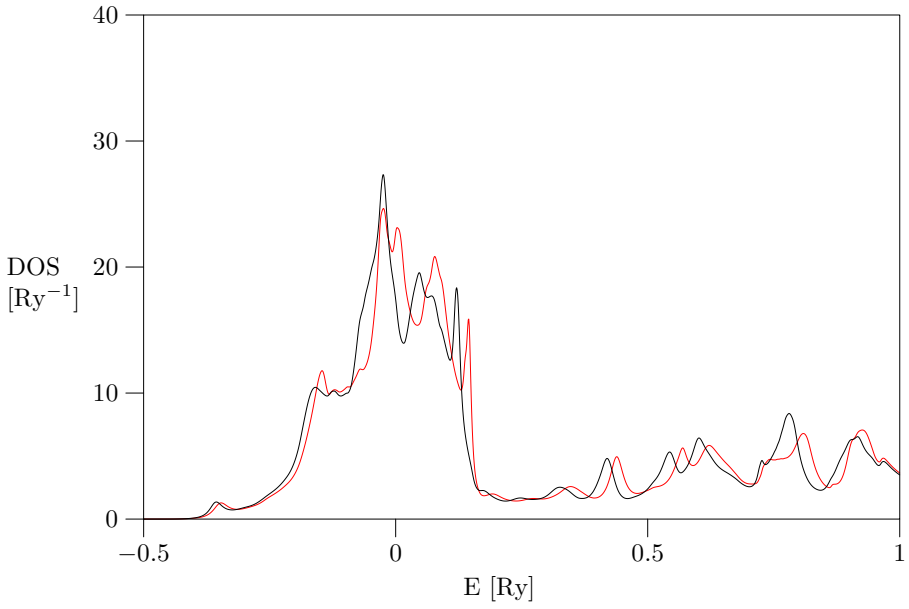

Figure 5.8: Density of states on centeral atom of single layer tip containing 25 atoms. The layer is diamond shape with each side formed by 5 atoms. Data are shown before (black) and after (red) self-consistent procedure.

Chapter 6

Current

In this chapter we calculate transport properties of atomic wires of various shapes similar to the system shown schematically in Fig. 1.1. Our model system mostly consists of two semi-infinite electrodes connected to a gold atomic wire or atom contact as the central part. There would be no fundamental problem to replace the gold wire with a different metal, this lies merely in a change of the tight-binding parameters and thus different central Hamiltonian. It would also be possible to replace the central Hamiltonian with some molecular Hamiltonian at the DFT level to simulate transport through single-molecule junction.

6.1 Systems

We use the Hamiltonian as in equation 4.1. The left and right leads are in calculation replaced by their Green's functions. We can study differences between the conductances of different wires, especially the influence of the shape of the tip. The Green's function of the right surface is taken to be the same as for the left lead but it has to be transformed because of inversion that changes signs according to parity.

In the equilibrium we can use the equilibrium Green's functions. The local density of states on each atom can be calculated from the retarded Green's function of the central part in each step of the run of the self-consistent procedure that shifts the local potentials to ensure the local charge neutrality condition (see sect. 2.2.1).

Out of the equilibrium we use the equation 3.16 to calculate the local charges. The shift potentials have to be calculated for each bias separately. There are two basic variants of the charge self-consistent calculation. First, we can calculate the local charge density on each atom separately and second, as was used by Brandbryge *et al.* (1999), we can sum charges in one layer and use the same value of the shift potential for all the atoms in that layer. While the first approach is rather more physical, the latter allows more straightforward connection with the decrease of the external potential throughout the device. Realistic DFT calculations usually suppose charge neutrality of the whole central region.

The transmission function can be then calculated using the equation 3.17 and the current by integration of this function over the window of energies allowed by the Fermi levels (Eq. 3.18).

We again suppose layered structure of the contact with triangular layers. Our notation of the contact with N layers is similar to the notation of the tips: a set of number gives number of rows (that is, the number atoms in one side of the triangle) starting from the left surface to the right surface. The layers are numbered from one to N, the left (right) surface is marked 0 ($N+1$) in the figures. When a part of the contact has structure of an atomic wire then the atoms lie in a line perpendicular to surface (like in Fig. 1.1).

6.2 Results

We calculated transmission functions of various systems – atomic contact, atomic wires and single level molecular quantum dots.

We use a simple method to find the transmission eigenvalues based on the method of powers. This iterative method searches for an eigenvector with the largest eigenvalue. To find eigenvectors with smaller eigenvalues we need to project the transmission matrix T on a subspace of the Hilbert space that do not include the found eigenvector. If the method finds eigenvector $|i\rangle$ then we project the subspace of this vector out with the projection operator $\mathcal{P} = 1 - |i\rangle\langle i|$, so that the new transmission matrix is $T' = \mathcal{P}T\mathcal{P}$. Now we can use again the method to find the second highest eigenvalue.

6.2.1 Transmission functions

We calculated transmission functions of various systems without the charge self-consistent method. Again, we used only the diagonal blocks of the surface Green's function to calculate the coupling and the transmission.

We present transmission functions for three atom wire 1-1-1 in equilibrium (Fig. 6.1) and with applied bias 0.05 Ry (0.68 eV) (fig 6.2). The transmission function ranges between 0.6 and 1.0 in the interval of energies around the Fermi energy in both cases. These values are in agreement with previous calculations and experiments. We can argue that the transmission is dominated by the s-electrons for energies between approximately 0.1 Ry and the Fermi energy 0.285 Ry. For energies higher than the Fermi energy p-electrons seem to have effect.

Transmission function for the atom contact in equilibrium is shown in Fig. 6.3. Local density of states projected on the orbitals of the central atom are plotted with dashed lines. This system consists of two tips 3-2-1 on left and right surfaces that share the apex atom, so that in our notation we can write 3-2-1-2-3. The structure is more complex than for the three atom wire with unexpectedly low transmission under the Fermi energy. However, as was shown in the previous chapter, the local shift potential on the apex atom was nearly 0.1 Ry so that the transmission after the self-consistent is expected to change.

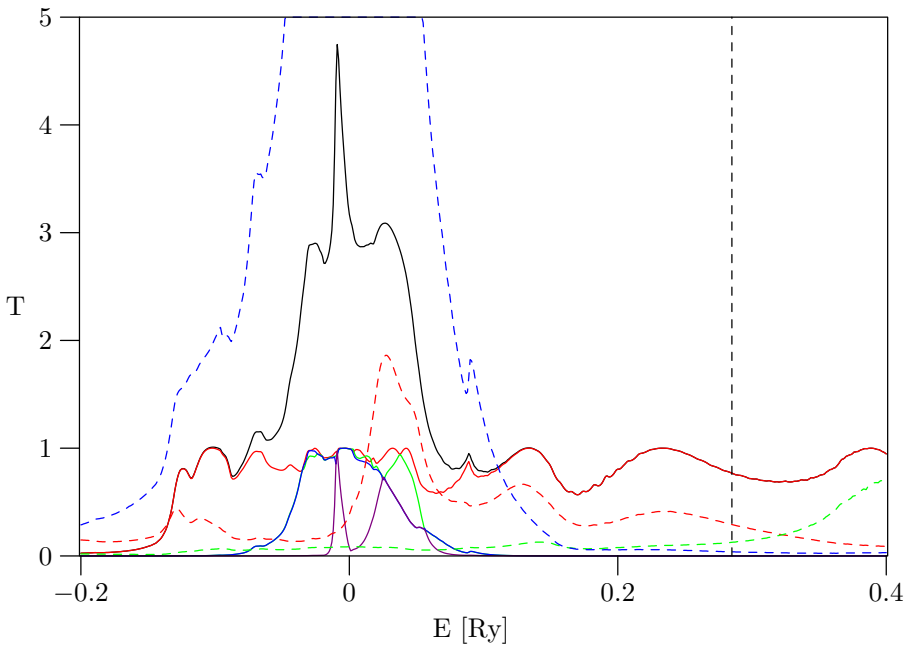

Figure 6.1: Transmission function of three atom wire between two leads. Total transmission function (black) and the four transmission eigenvalues are shown with full lines. Dashed lines show local density of states in the wire: s-states with red, p-states with green and d-states with blue dashed line. The LDOS were multiplied by a factor of 0.2.

6.2.2 Self-consistent calculation

As was shown in the previous chapter, the self-consistent procedure has a significant effect on atoms on the surface of the tip. Therefore we run this procedure for three systems under different biases. The systems were the atomic contact (3-2-1-2-3) and two atomic wires with three and six atoms between the tips. The procedure also allows us to roughly calculate the potential drop along the wire. This is obtained by comparison of the local potentials for wire without and with the bias. However, as we use many approximations the drop might be slightly different for a real device.

Our calculations show that the differences between the local potentials in one layer are small. Therefore, the results obtained from the local charge neutrality and layer charge neutrality methods should be similar.

The local potentials and potential differences for atomic contact under different biases from 0.0 Ry up to 0.2 Ry are shown in Fig. 6.4 and 6.5. We can see that the potential is nearly symmetric and the local potential shift remains almost the same for the central atom of the contact.

The local shift potential and their differences for different biases up to 0.2 Ry for contact 3-2-1-1-1-2-3 are in Fig. 6.6 and 6.7. In this case the potential drop is not symmetric but occurs near the first atom of the wire, i.e. between the second layer and the central atom

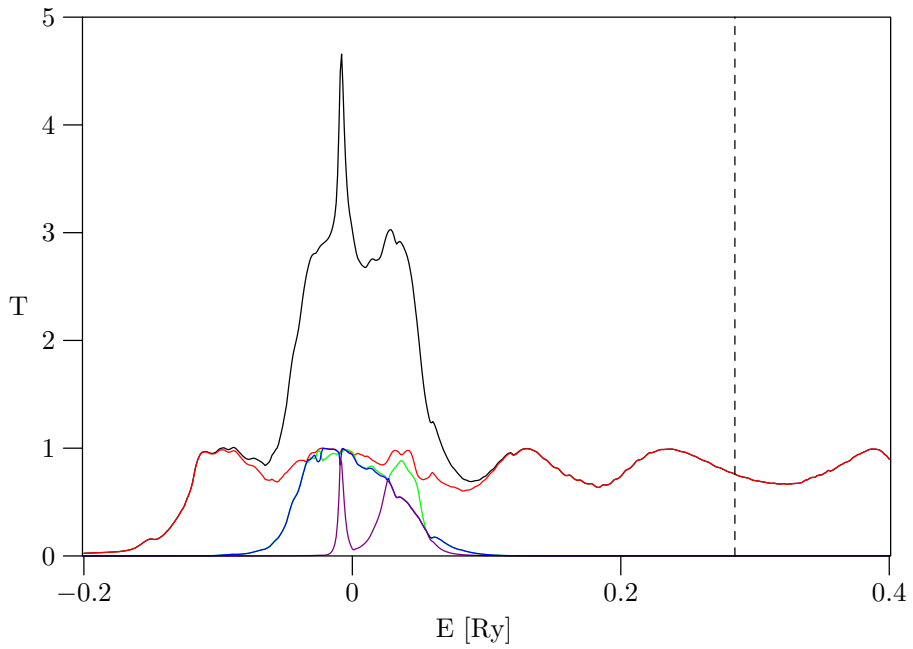

Figure 6.2: The transmission function of three atom wire under bias 0.050Ry. Total transmission function (black) and the four transmission eigenvalues are shown.

of the wire.

The self-consistent procedure for atomic wire with 6 atoms is time-consuming and it is difficult to obtain converged local shift potentials. The calculation with roughly converged local potential shifts shows a zero-bias conductivity equal to the quantum unit.

Zero-bias transmission function for 3-2-1-1-1-2-3 atomic wire is shown in Fig. 6.8. It shows unit conductance at the Fermi energy and a set of sharp peaks between 0.1 and 0.2 that come from the localized d states in the wire.

The presented results should be viewed rather as a qualitative. There is no spatial relaxation in our model, we use bulk interatomic distances for the atoms in the wire. Despite of this, the calculated zero-bias conductance is near the quantum unit which is in agreement with experiments and previous calculations.

6.3 Molecular single level Hamiltonians

The presented procedure allows us to insert arbitrary Hamiltonian to the central part. Organic molecules with conjugated bonds have delocalized π orbitals at energies near the Fermi level. These orbitals span along the molecule allowing transmitting electron to pass. These states can be simulated by model Hamiltonian as one state between the leads in the central part. This way we obtain transmission function that qualitatively correspond with transmission function of a simple molecule with one resonant state. However, real

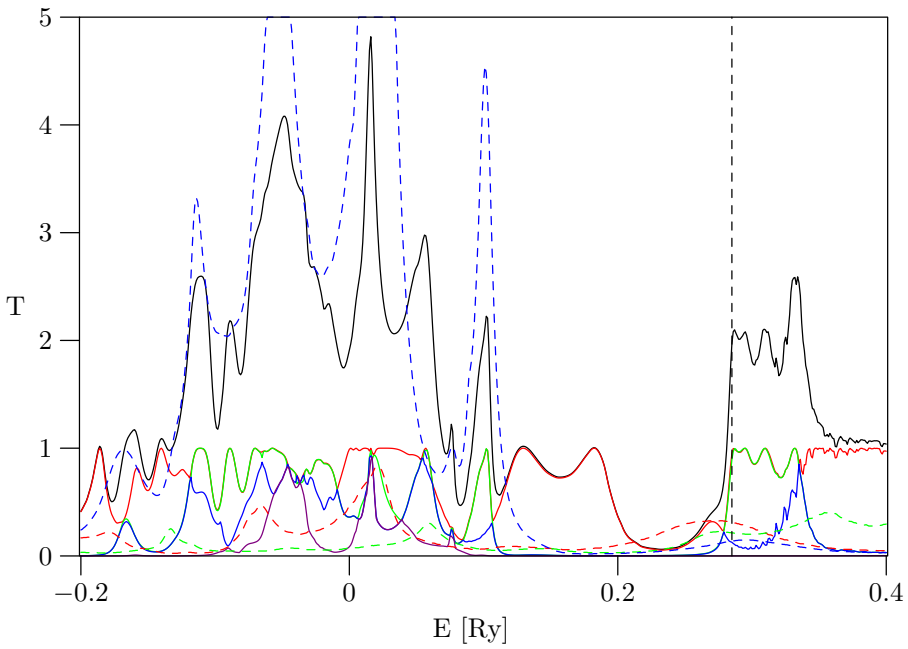

Figure 6.3: The transmission function of atomic contact without charge equilibration. Total transmission function (black) and the four transmission eigenvalues are shown. The plot shows density of states on the contact atom with dashed lines. s-states with red, p-states with green and d-states with blue dashed line. The LDOS were multiplied by a factor of 0.2.

molecules have more states near the Fermi energy so that the electron has more possibilities to pass. The equation 3.17 for one level with constant coupling to each orbital on both sides reads

$$T(E) = \frac{\Gamma_L(E - V/2)\Gamma_R(E + V/2)}{(E - E_M - \Delta)^2 + \frac{1}{4}(\Gamma_L(E - V/2) + \Gamma_R(E + V/2))^2}\,, \tag{6.1}$$

where E_M is energy of the level and Δ is the hermitian part of the total self-energy, the anti-hermitian coupling Γ is directly connected to the density of states of the tip that we calculated in the previous chapter. This equation is widely used in wide-band limit calculations, in which case the Γ is energy-independent and the transmission is Lorentzian function. In contrast, we use energy-dependent self-energies (and therefore energy-dependent Γ). In this case the transmission function can vary a lot for different biases depending on the density of states on the atoms in contact with the single level.

Transmission functions for a simple one level system under different biases is shown in Fig. 6.9. We took a Hamiltonian of a 1-1-1 system and replaced the central atom with one level that coupled only to the s and $3z^2 - r^2$ states of the two neighbouring atoms. We also "switched off" the interaction and overlap between the first and last atoms of the wire. We can see that the energy-dependent self-energy causes another peaks in the transmission function.

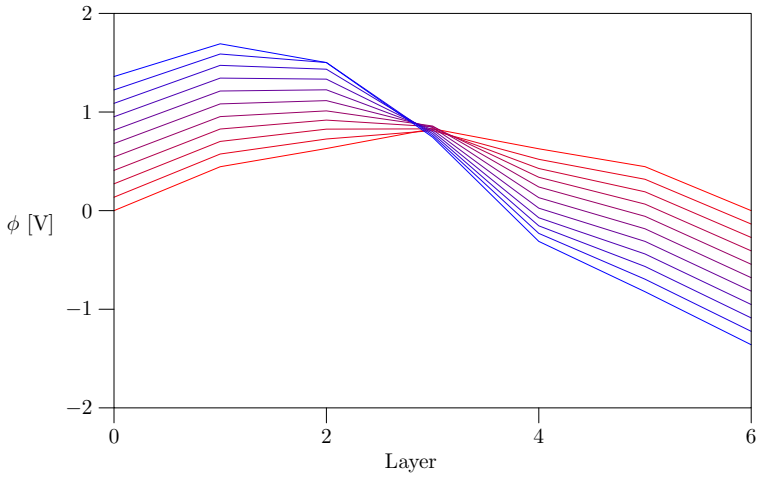

Figure 6.4: Local shift potentials for layers of atomic contact. Surfaces are connected with two 3-2-1 tips that share the apex atom. Bias voltage ranged from 0.0 Ry to 0.2 Ry (2.72 V, blue line). Layers 0 and 6 represent the left and right surfaces.

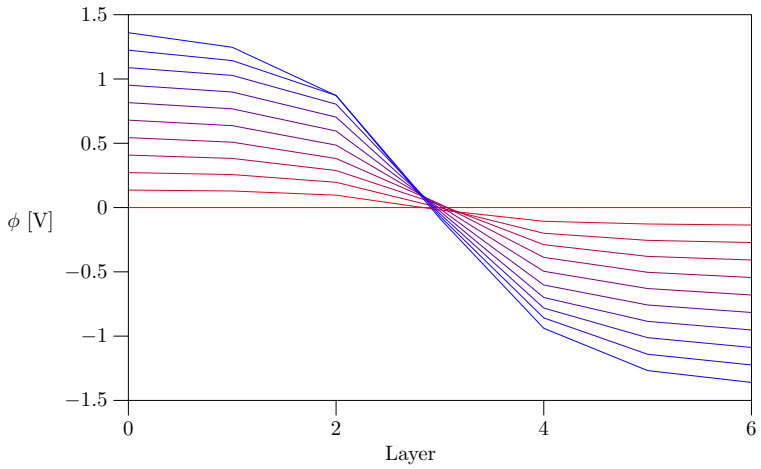

Figure 6.5: Change of the local shift potentials from the zero-bias shift potential for layers of atomic contact system. The data represent the difference $\phi_i(V) - \phi_i(0)$, where V is the applied bias and i is the index of layer.

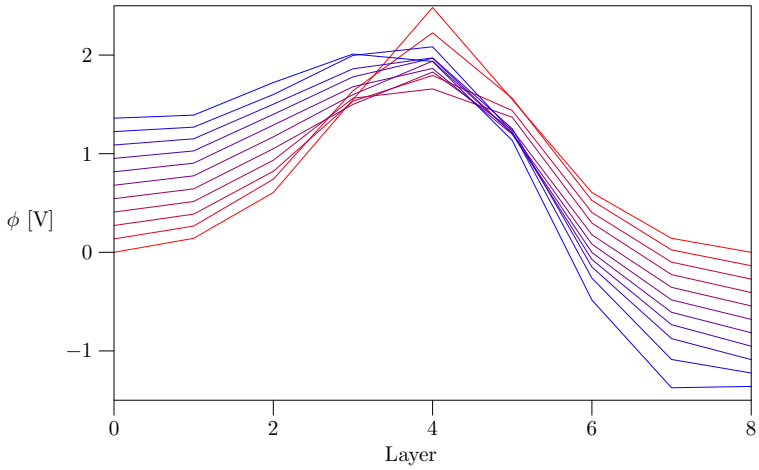

Figure 6.6: Local shift potentials for layers of a simple atomic wire. Surfaces are connected with two 3-2-1 tips that are connected with another atom (geometry 3-2-1-1-1-2-3). Bias voltage ranged from 0.0 Ry (red line) to 0.2 Ry (2.72 V, blue line). Layers 0 and 8 represent the left and right surfaces.

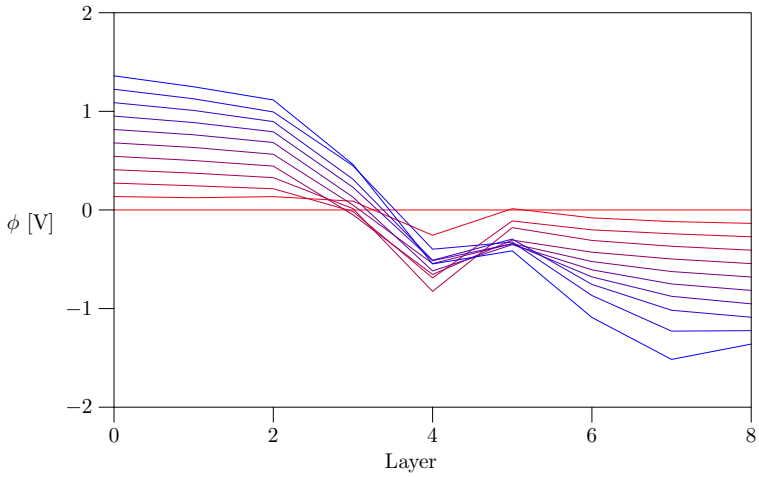

Figure 6.7: Difference between the local shift potential with applied bias and without the bias. The bias changed from 0.0 Ry (red line) to 0.2 Ry (blue line). Same system as in Fig. 6.6.

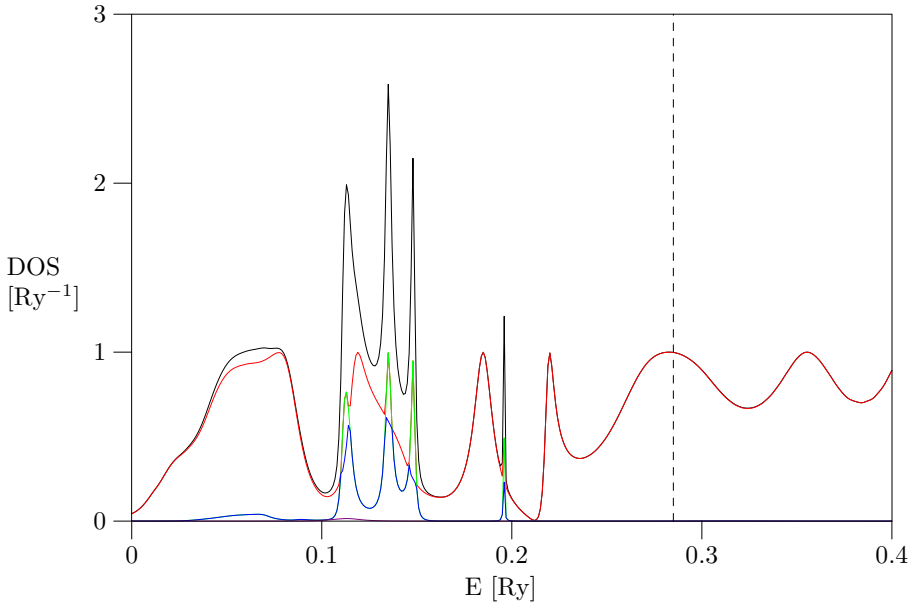

Figure 6.8: Transmission function of the 3-2-1-1-1-2-3 system after charge self-sonsistent procedure. Position of the Fermi energy is marked with the vertical dashed line.

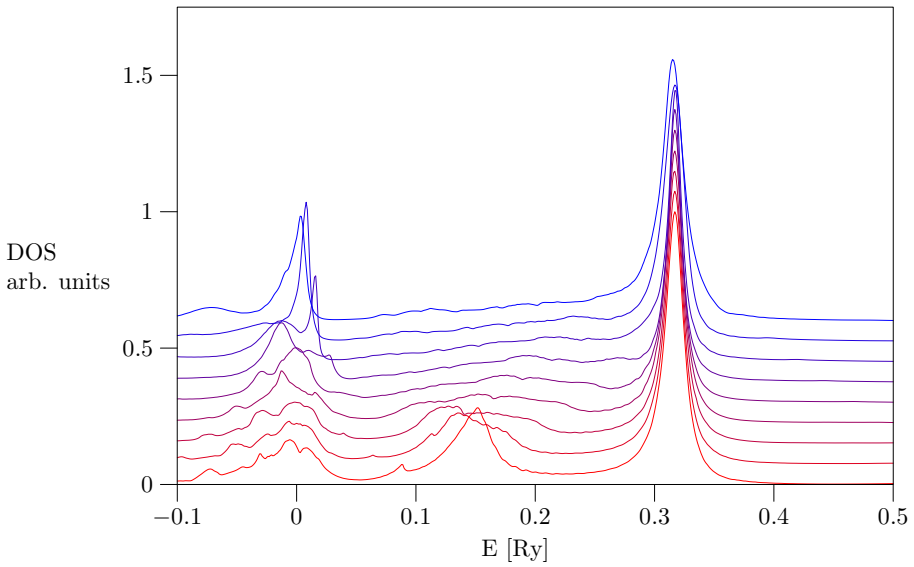

Figure 6.9: Transmission function of one level device for various biases ranging from 0.0 Ry to 0.4 Ry. The central atom of a 1-1-1 contact was replaced with a state with energy $E = E_F$. This state coupled to the s and $3z^2 - r^2$ states of the first and last atoms of the wire. The value of the interaction was taken weaker than for two s orbitals in the same distance.

Chapter 7

Conclusions

In this work we presented a method for calculations of electronic properties of atomic clusters (tips) connected to the surface of a lead (electrode) based on a calculation of the surface Green's function of the lead. Using our implementation of this method we studied differences between local electronic densities of states (LDOS) on apex atoms of various tips. We were interested in this quantity because it is important for the transport properties of molecular junctions and has a significant effect on the conduction, peak in the LDOS aligned with the Fermi energy can change the magnitude of the conduction by an order or more. It was found that the changes in the LDOS are significant for sharp tetrahedron tips and less important for blunt tips because the apex local density of states is flattened in those tips.

We also studied the impact of different approximations of the surface Green's function on the tip density of states. We compared the tight-binding surface Green's function and surface in the wide-band limit (WBL) that assumes energy-independent density of states for the surface and is widely used for calculation of inelastic effects. We showed that the LDOS calculated using the realistic surface Green's function differs substantially from the LDOS calculated in the WBL, for example, it shifts the location of the peaks.

The charge self-consistent tight binding (SCTB) procedure was implemented to improve our calculations. This method is used to find local shift potentials that are added to the Hamiltonian to ensure local charge neutrality. The implementation of this method was used in the calculation of electronic properties of the tips. As we anticipated, the local shift potentials have considerable effect on LDOS of atoms without some of their neighbours, e.g. the apex atom.

We implemented method that allows calculations of transmission functions of gold clusters connecting two surfaces (contacts) based on the Green's functions formalism. To test this method we calculated transmission functions of various systems without application of the SCTB method. With the use of the SCTB method we calculated the local potential shifts for different contacts. This allowed us to approximately determine the potential drop along the contact. Results of our calculations correspond with the results of previous works, we reproduced the conductance of one conductance quantum at the Fermi energy for short atomic wire in accordance with experiments and more sophisticated calculations

using DFT (Mozos *et al.* (2002)).

In our calculations we used only a part of the surface Green's function. For future calculations it would be important to add more blocks of the Green's function to assess their importance. The implemented methods can be also used with *ab initio* Hamiltonian that would improve the quality of the results.

The results of the presented work for the surface Green's functions are used as an input for calculations of molecular conductance including the interactions of transmitted electrons with the molecular vibrations. This work, extending the paper of Benesch *et al.* (2006) will be published in near future.

Appendix A

Non-orthogonal basis

In this section we shall summarize the results obtained for non-orthogonal basis set. Let $|i\rangle$ be a basis of normalized functions with symmetric overlap matrix

$$\langle i|j\rangle = S_{ij}\,. \tag{A.1}$$

Let $|i^o\rangle$ be an orthonormal basis that spans the same part of Hilbert space, and

$$\langle i^o|j\rangle = T_{i^o j} \tag{A.2}$$

is the overlap between the two basis sets.

Now for $|j\rangle$ we readily have

$$|j\rangle = \sum_{i^o} |i^o\rangle\langle i^o|j\rangle = \sum_{i^o} T_{i^o j}|i^o\rangle\,. \tag{A.3}$$

Let us suppose that there is a matrix O that transforms the non-orthogonal basis to the orthogonal

$$|i^o\rangle = \sum_l O_{li^o}|l\rangle\,. \tag{A.4}$$

Taking matrix elements we have

$$\langle k|i^o\rangle = \sum_l O_{li^o}\langle k|l\rangle \tag{A.5}$$

$$\{T_{i^o k}\}^* = \sum_l O_{li^o} S_{kl} \tag{A.6}$$

$$\sum_k S^{-1}_{jk}\langle k|i^o\rangle = O_{ji^o}\,, \tag{A.7}$$

therefore the orthonormal basis element

$$|i^o\rangle = \sum_{kl} S^{-1}_{lk}\langle k|i^o\rangle|l\rangle\,. \tag{A.8}$$

The ... relation in the non-orthogonal basis

$$\mathcal{I} = \sum_{i^o} |i^o\rangle\langle i^o| = \sum_{i^o klmn} S^{-1}_{lk}\langle k|i^o\rangle|l\rangle\langle m|\langle i^o|n\rangle S^{-1}_{mn} = \tag{A.9}$$

$$= \sum_{klmn} |l\rangle S^{-1}_{lk}\langle k|n\rangle S^{-1}_{nm}\langle m| = \sum_{lm} |l\rangle S^{-1}_{lm}\langle m| \tag{A.10}$$

One particle operator in basis $|i\rangle$

$$\hat{A} = \sum_{klmn} |k\rangle S^{-1}_{kl}\langle l|\hat{A}|m\rangle S^{-1}_{mn}\langle n| = \sum_{klmn} |k\rangle S^{-1}_{kl} A_{lm} S^{-1}_{mn}\langle n| = \sum_{kn} |k\rangle \mathcal{A}_{kn}\langle n|\,, \tag{A.11}$$

where

$$\mathcal{A}_{kn} = \sum_{lm} S^{-1}_{kl} A_{lm} S^{-1}_{mn}\,. \tag{A.12}$$

The trace operator

$$\mathrm{Tr}\hat{A} = \sum_{i^o}\langle i^o|\hat{A}|i^o\rangle = \sum_{i^o ijkl}\langle i^o|k\rangle S^{-1}_{kl}\langle l|A|i\rangle S^{-1}_{ij}\langle j|i^o\rangle = \tag{A.13}$$

$$= \sum_{ijkl} S_{jk} S^{-1}_{kl} A_{li} S^{-1}_{ij} = \sum_{il} A_{li} S^{-1}_{il} \tag{A.14}$$

using eq above we have

$$\mathrm{Tr}\hat{A} = \sum_{kn} \mathcal{A}_{kn} S_{nk} = \mathrm{Tr}\mathcal{A}S\,. \tag{A.15}$$

The Green's function obeys the relation

$$(E\mathcal{I} - H)G(E) = \mathcal{I}\,, \tag{A.16}$$

inserting $G = \sum_{ij} |i\rangle\mathfrak{g}_{ij}(E)\langle j|$ and taking matrix element we obtain

$$\langle k|(E\mathcal{I} - H)\sum_{ij} |i\rangle\mathfrak{g}_{ij}(E)\langle j|l\rangle = \langle k|l\rangle \tag{A.17}$$

$$\sum_{ij}(ES_{ki} - H_{ki})\mathfrak{g}_{ij}(E)S_{jl} = S_{kl} \tag{A.18}$$

$$\sum_{i}(ES_{ki} - H_{ki})\mathfrak{g}_{in}(E) = \delta_{kn} \tag{A.19}$$

The density of states is

$$\varrho = -\frac{1}{\pi}\Im\mathrm{m}\mathrm{Tr}G = -\frac{1}{\pi}\Im\mathrm{m}\mathrm{Tr}\mathfrak{g}S\,. \tag{A.20}$$

Bibliography

Agraït N., Rodrigo J. G. and Vieira S. (1993): *Conductance steps and quantization in atomic-size contacts*, Phys. Rev. B **47**, 12 345–12 348.

Agraït N., Untiedt C., Rubio-Bollinger G. and Vieira S. (2002): *Onset of Energy Dissipation in Ballistic Atomic Wires*, Phys. Rev. Lett. **88**, 216803.

Artacho E. and del Bosch L. M. (1991): *Nonorthogonal basis sets in quantum mechanics: Representations and second quantization*, Phys. Rev. A **43**, 5770–5777.

Aviram A. and Ratner M. A. (1974): *Molecular rectifiers*, Chem. Phys. Letters **29**, 277–283.

Benesch C., Čížek M., Thoss M. and Domcke W. (2006): *Vibronic Effects on Resonant Electron Conduction through Single Molecule Junctions*, Chem. Phys. Lett. **430**, 355.

Binning G., Rohrer H., Gerber Ch. and Weibel E. (1982): *Surface Studies by Scanning Tunneling Microscopy*, Phys. Rev. Lett. **49**, 57–61.

Bockrath M., Cobden D. H., McEuen P. L., Chopra N. G., Zettl A., Thess A. and Smalley R. E. (1997): *Single-Electron Transport in Ropes of Carbon Nanotubes*, Science **275**, 1922–1925.

Brandbyge M., Kobayashi N. and Tsukada M. (1999): *Conduction channels at finite bias in single-atom gold contacts*, Phys. Rev. B **60**, 17 064–17 070.

Bratkovsky A. M., Sutton A. P. and Todorov T. N. (1995): *Conditions for conductance quantization in realistic models of atomic-scale metallic contacts*, Phys. Rev. B **52**, 5036–5046.

Bumm L. A., Arnold J. J., Cygan M. T., Dunbar T. D., Burgin T. P., Jones L., Allara D. L., Tour J. M. and Weiss P. S. (1996): *Are Single Molecular Wires Conducting?*, Science **271**, 1705–1707.

Bumm L. A., Arnold J. J., Dunbar T. D., Allara D. L. and Weiss P. S. (1999): *Electron Transfer through Organic Molecules*, J. Phys. Chem. B **103**, 8122–8127.

Cuevas J. C., Levy Yeyati A. and Martín-Rodero A. (1998): *Microscopic Origin of Conducting Channels in Metallic Atomic-Size Contacts*, Phys. Rev. Lett. **80**, 1066–1069.

Dreher M., Pauly F., Heurich J., Cuevas J. C., Scheer E. and Nielaba P. (2005): *Structure and conductance histogram of atomic-sized Au contacts*, Phys. Rev. B **72**, 075435.

Drexler K. E. (1981): *Molecular engineering: An approach to the development of general capabilities for molecular manipulation*, Proc. Natl. Acad. Sci. USA, (September), 78:5275-5278.

Dürig U., Züger O. and Pohl D. W. (1990): *Observation of Metallic Adhesion Using the Scanning Tunneling Microscope*, Phys. Rev. Lett. **65**, 349-352.

Economou E. N. (1983): *Green's Functions in Quantum Physics*, Springer-Verlag, Berlin.

Fetter A. L. and Walecka J. D. (1971): *Quantum Theory of Many-Particle Systems*, McGraw-Hill, New York.

Frank S., Poncharal P., Wang Z. L. and de Heer W. A. (1998): *Carbon Nanotube Quantum Resistors*, Science **280**, 1744–1746.

Frederiksen T., Brandbyge M., Lorente N. and Jauho A-P. (2004): *Inelastic Scattering and Local Heating in Atomic Gold Wires*, Phys. Rev. Lett. **93**, 256601.

Gimzewski J. K. and Möller R. (1987): *Transition from the Tunneling Regime to Point Contact Studied using Scanning Tunneling Microscopy*, Phys. Rev. B **36**, 1284–1287.

Goringe C. M., Bowler D. R. and Hernández E. (1997): *Tight-binding modelling of materials*, Rep. Prog. Phys. **60**, 1447–1512.

Hansma P. K. (1977): *Inelastic electron tunneling*, Phys. Rep. 30 **2**, 145–206.

Haug H. and Jauho A.-P. (1996): *Quantum Kinetics in Transport and Optics of Semiconductors*, Springer.

Heath J. R. and Ratner M. A. (2003): *Molecular electronics*, Physics Today, (May) 43–49.

Hirose K. and Tsukada M. (1995): *First-principles calculation of the electronic structure for a bielectrode junction system under strong field and current*, Phys. Rev. B **51**, 5278–5290.

Horsfield A. P., Bowler D. R., Fisher A. J., Todorov T. N. and Sánchez C G. (2005): *Correlated electron-ion dynamics: the excitation of atomic motion by energetic electrons*, J. Phys.: Condens. Matter **17**, 4793–4812.

Jansen A. G. M., van Gelder A. P. and Wyder P. (1980): *Point-contact spectroscopy in metals*, J. Phys. C: Solid St. Phys. **13** 6073.

Jauho A-P., Wingreen N. S. and Meir Y. (1994): *Time-dependent transport in interacting and noninteracting resonant-tunneling systems*, Phys. Rev. B **50**, 5528–5544.

Jelínek P., Pérez R., Ortega J. and Flores F. (2003): *First-principles simulations of the stretching and final breaking of Al nanowires: Mechanical properties and electrical conductance*, Phys. Rev. B **68**, 085403.

Joachim C. and Gimzewski J. K. (1995): *Electronic Transparence of a Single C_60 Molecule*, Phys. Rev. Lett. **74**, 2102–2105.

Joachim C. and Gimzewski J. K. (1997): *An electromechanical amplifier using a single molecule*, Chem. Phys. Lett. **265**, 353–357.

Krans J. M., Muller C. J., Yanson I. K., Govaert Th. C. M., Hesper R. and van Ruitenbeek J. M. (1993): *One-atom point contacts*, Phys. Rev. B **48**, 14721–14724.

Lake R., Klimeck G., Bowen R. C. and Jovanovic D. (1997): *Single and multiband modeling of quantum electron transport through layered semiconductor devices*, J. Appl. Phys. **81** (12), 7845–7869.

Landauer R. (1970): *Electrical resistence of disordered one-dimensional lattices*, Philos. Mag. **21**, 863.

Lang N. D. (1995): *Resistance of atomic wires*, Phys. Rev. B **52**, 5335–5342.

Langlais V. J., Schlittler R. R., Tang H., Gourdon A., Joachim C. and Gimzewski J. K. (1999): *Spatially Resolved Tunneling along a Molecular Wire*, Phys. Rev. Lett. **83**, 2809–2812.

Liang G. C., Ghosh A. W., Paulsson M. and Datta S. (2004): *Electrostatic potential profiles of molecular conductors*, Phys. Rev. B **69**, 115302.

López Sancho M. P., López Sancho J. M. and Rubio J. (1984): *A non-orthogonal-basis calculation of the spectral density of surface states for the (100) and (110) faces of tungsten*, J. Phys. C.: Solid State Phys. **18**, 1803–1815.

López Sancho M. P., López Sancho J. M. and Rubio J. (1985): *Highly convergent schemes for the calculation of bulk and surface Green functions*, J. Phys. F: Met. Phys **15**, 851–858.

Mehl M. J. and Papaconstantopoulos D. A. (1996): *Applications of a tight-binding total-energy method for transition and noble metals: Elastic constants, vacancies, and surfaces of monatomic metals*, Phys. Rev. B **54**, 4519–4530. The parameters can be downloaded from: http://cst-www.nrl.navy.mil/bind/

Meir Y. and Wingreen N. S. (1992): *Landauer Formula for the Current through an Interacting Electron Region*, Phys. Rev. Lett. **68**, 2512–2515.

Mozos J. L., Ordejón P., Brandbyge M., Taylor J. and Stokbro K. (2002): *Simulations of quantum transport in nanoscale systems: application to atomic gold and silver wires*, Nanotechnology **13**, 346–351.

Mujica V., Kemp M. and Ratner M. A. (1994): *Electron conduction in molecular wires. I. A scattering formalism*, J. Chem. Phys. **101** (8), 6849–6855.

Muller C. J., van Ruitenbeek J. M. and de Longh L. J. (1992a): *Experimental observation of the transition from weak link to tunnel junction*, Physica C **191**, 485–504.

Muller C. J., van Ruitenbeek J. M. and de Longh L. J. (1992b): *Conductance and Supercurrent Discontinuities in Atomic-Scale Metallic Constrictions of Variable Width*, Phys. Rev. Lett. **69**, 140–143.

Ness H., Shevlin S. A. and Fisher A. J. (2001): *Coherent electron-phonon coupling and polaronlike transport in molecular wires* Phys. Rev. B **63**, 125422.

Nielsen S. K., Brandbyge M., Hansen K., Stokbro K., van Ruitenbeek J. M. and Besen-

bacher F. (2002): *Current-Voltage Curves of Atomic-Sized Transition Metal Contacts: An Explanation of Why Au is Ohmic and Pt is Not*, Phys. Rev. Lett. **89**, 066804.

Nitzan A. (2001): *Electron transmission Through Molecules and Molecular Interfaces*, Annu. Rev. Phys. Chem. **52**, 681–750.

Nitzan A. and Ratner M. A. (2003): *Electron transport in Molecular Wire Junctions*, Science, **300**, 1384–1389.

Paulsson M., Frederiksen T. and Brandbyge M. (2005): *Modeling inelastic phonon scattering in atomic- and molecular-wire junctions*, Phys. Rev. B **72**, 201101.

Persson B. N. J. and Baratoff A. (1987): *Inelastic Electron Tunneling from a Metal Tip: The Contribution from Resonant Processes* Phys. Rev. Lett. **59**, 339–342.

Priyadarshy S., Skourtis S. S., Risser S. M. and Beratan D. N. (1996): *Bridge-mediated electronic interactions: Differences between Hamiltonian and Green function partitioning in a non-orthogonal basis*, J. Chem. Phys **104** (23), 9473–9481.

Reed M. A., Zhou C., Muller C. J., Burgin T. P. and Tour J. M. (1997): *Conductance of a Molecular Junction*, Science **278**, 252–254.

Sánchez C. G., Stamenova M., Sanvito S., Bowler D. R., Horsfield A. P. and Todorov T. N. (2006): *Molecular conduction: Do time-dependent simulations tell you more than the Landauer approach?*, The J. of Chem. Phys. **124**, 214708.

Sergueev N., Roubtsov D. and Guo H. (2005): *Ab initio Analysis of Electron-Phonon Coupling in Molecular Devices* Phys. Rev. Lett. **95**, 146803.

Slater J. C. and Koster G. F. (1954): *Simplified LCAO Method for the Periodic Potential Problem*, Phys. Rev. **94**, 1498–1524.

Stipe B. C., Rezaei M. A. and Ho W. (1998): *Single-Molecule Vibrational Spectroscopy and Microscopy*, Science **280**, 1732–1735.

Stokbro K., Taylor J., Brandbyge M. and Guo H. (2005): *Ab-initio Non-Equilibrium Green's Function formalism for calculating electron transport in molecular devices*, in *Introducing Molecular Electronics*, Springer Lecture notes in Physics **680** 117–151.

Tans S. J., Verscheuren A. R. M. and Dekker C. (1998): *Room-temperature transistor based on a single carbon nanotube*, Nature **393**, 49–52.

Taylor J., Guo H. and Wang J. (2001): *Ab initio modeling of quantum transport properties of molecular electronic devices*, Phys. Rev. B **63**, 245407.

Thygesen K. S. (2006): *Electron transport through an interacting region: The case of a nonorthogonal basis set*, Phys. Rev. B **73**, 035309.

Velev J. and Butler W. (2004): *On the equivalence of different techniques for evaluating the Green function for a semi-infinite system using a localized basis*, J. Phys.: Condens. Matter **16**, R637–R657.

Xue Y., Datta S. and Ratner M. A. (2002): *First-principles based matrix Green's function approach to molecular electronic devices: general formalism*, Chem. Phys. **281**, 151–

170.

Xue Y. and Ratner M. A. (2003): *Microscopic study of electrical transport through individual molecules with metallic contacts.* I. *Band lineup, voltage drop and high-field transport*, Phys. Rev. B **68**, 115406.

Zahid F., Paulsson M. and Datta S. (2003): *Electrical Conduction through Molecules* in *Advanced Semiconductors and Organic Nano-Techniques*, edited by H. Morkoc, Academic Press.

Zhou C., Kong J. and Dai H.: *Intrinsic Electrical Properties of Individual Single-Walled Carbon Nanotubes with Small Band Gaps*, Phys. Rev. Lett. **84** (2000) 5604–5607.